





**STATISTICAL-THERMAL MODEL DESCRIPTION of HADRON YIELDS  
in HIGH ENERGY COLLISIONS**

**M.Sc. THESIS**

**Çiğdem YAŞAR**

**Department of Physics Engineering**

**Physics Engineering Programme**

**MAY 2014**



**STATISTICAL-THERMAL MODEL DESCRIPTION of HADRON YIELDS  
in HIGH ENERGY COLLISIONS**

**M.Sc. THESIS**

**Çiğdem YAŞAR  
(509121103)**

**Department of Physics Engineering**

**Physics Engineering Programme**

**Thesis Supervisor: Prof. Dr. Cenap Şahabettin ÖZBEN**

**MAY 2014**



**İSTANBUL TEKNİK ÜNİVERSİTESİ ★ FEN BİLİMLERİ ENSTİTÜSÜ**

**YÜKSEK ENERJİLİ ÇARPIŞMALARDA OLUŞAN ÜRÜN MİKTARLARININ  
İSTATİSTİKSEL TERMAL MODEL YÖNTEMİYLE  
İNCELENMESİ**

**YÜKSEK LİSANS TEZİ**

**Çiğdem YAŞAR  
(509121103)**

**Fizik Mühendisliği**

**Fizik Mühendisliği**

**Tez Danışmanı: Prof. Dr. Cenap Şahabettin ÖZBEN**

**MAYIS 2014**



**Çiğdem YAŞAR**, a M.Sc. student of ITU Institute of Science and Technology 509121103 successfully defended the thesis entitled “**STATISTICAL-THERMAL MODEL DESCRIPTION of HADRON YIELDS in HIGH ENERGY COLLISIONS**”, which she prepared after fulfilling the requirements specified in the associated legislations, before the jury whose signatures are below.

**Thesis Advisor :**      **Prof. Dr. Cenap Şahabettin ÖZBEN** .....  
Istanbul Technical University

**Co-advisor :**            **Asst. Prof. Dr. Ayben Karasu Uysal** .....  
KTO Karatay University

**Jury Members :**        **Assoc. Prof. Dr. Kerem Cankoçak** .....  
Istanbul Technical University

**Assoc. Prof. Dr. Hakkı Tunçay Özer** .....  
Istanbul Technical University

**Prof. Dr. Serkant Ali Çetin** .....  
Doğuş University

**Date of Submission :**    **5 May 2014**

**Date of Defense :**        **30 May 2014**



*To my dear parents,*



## FOREWORD

I would like to thank to my advisor Prof. Dr. Cenap Şahabettin ÖZBEN for his unconditional support for my thesis and for giving me a chance to work with Yrd. Doç. Dr. Ayben Karasu UYSAL who is among the experts about my thesis subject.

I would like to thank Prof. Dr. Metin SUBAŞI for standing for me as a role model for his complete fairness and virtue, for showing me how to turn on the light inside me into a propulsive power for doing my best.

I would like to thank my co-advisor Yrd. Doç. Dr. Ayben Karasu UYSAL for giving me the right academic sense, extremely required for obtaining felicitous scientific outcome and her kind support and motivation particularly in the hard times.

I would like to thank my father Mustafa YAŞAR, my mother Rahime YAŞAR and my brother Mehmet YAŞAR for insistenty encouraging me for my carrier during my education.

I would like to thank my co-worker Esra BARLAS for her helpful discussions and suggestions when I was saturated.

I would like to thank The Scientific and Technological Research Council of Turkey (TÜBİTAK) for their financial support during my thesis study in the frame of 2211 National Graduate Scholarship Programme. I would also like to thank to TÜBİTAK again for accepting my participation to the 3501 National Young Researchers Career Development Programme as a volunteer researcher.

May 2014

Çiğdem YAŞAR  
(Physicist)



## TABLE OF CONTENTS

	<u>Page</u>
<b>FOREWORD</b> .....	<b>ix</b>
<b>TABLE OF CONTENTS</b> .....	<b>xi</b>
<b>ABBREVIATIONS</b> .....	<b>xiii</b>
<b>LIST OF TABLES</b> .....	<b>xv</b>
<b>LIST OF FIGURES</b> .....	<b>xvii</b>
<b>SUMMARY</b> .....	<b>xxi</b>
<b>ÖZET</b> .....	<b>xxiii</b>
<b>1. INTRODUCTION</b> .....	<b>1</b>
<b>2. THE STANDARD MODEL OF PARTICLE PHYSICS</b> .....	<b>3</b>
2.1 Quantum Chromodynamics.....	5
2.2 Quark-Gluon Plasma .....	6
2.3 Relativistic Collisions.....	8
2.3.1 Proton-proton collisions .....	8
2.3.2 Relativistic heavy-ion collisions.....	8
2.4 Previous Proton-Proton and Heavy-Ion Results .....	9
2.4.1 Spectra of STAR experiment .....	9
2.4.1.1 Proton-proton collisions.....	10
2.4.1.2 Gold-Gold collisions.....	10
2.5 Spectra of ALICE Experiment .....	11
2.5.1 Proton-proton collisions .....	11
2.5.2 Lead-Lead collisions .....	12
<b>3. THEORETICAL MODELS</b> .....	<b>13</b>
3.1 Statistical-Thermal Model .....	13
3.1.1 The grand canonical ensemble .....	14
3.1.2 The canonical ensemble .....	16
3.1.3 The strangeness canonical ensemble .....	18
3.2 THERMUS .....	21
3.3 SHARE .....	22
<b>4. ANALYSIS</b> .....	<b>25</b>
4.1 Statistical-Thermal Model Analysis of STAR Experiment .....	28
4.1.1 Proton-proton collisions .....	28
4.1.2 Deuterium-Gold collisions .....	29
4.1.3 Gold-Gold collisions .....	32
4.2 Statistical-Thermal Model Analysis of ALICE Experiment .....	37
4.2.1 Proton-proton collisions .....	37

4.2.2 Lead-Lead collisions ..... 38

**5. RESULTS ..... 43**

**6. CONCLUSION AND OUTLOOK..... 49**

**REFERENCES..... 51**

**CURRICULUM VITAE..... 57**

## ABBREVIATIONS

<b>ALICE</b>	: A Large Ion Collider Experiment
<b>AuAu</b>	: Gold-Gold
<b>B</b>	: Baryon quantum number
<b>CERN</b>	: The European Organization for Nuclear Research
<b>dAu</b>	: Deuterium-Gold
<b>DPM</b>	: Dual Parton Model
<b>GC</b>	: Grand Canonical
<b>HG</b>	: Hadron Gas
<b>LHC</b>	: Large Hadron Collider
<b>PbPb</b>	: Lead-Lead
<b>PDG</b>	: Particle Data Group
<b>pp</b>	: Proton-Proton
<b>pQCD</b>	: Perturbative Quantum Chromodynamics
<b>Q</b>	: Charge quantum number
<b>QCD</b>	: Quantum Chromodynamics
<b>QGP</b>	: Quark-Gluon Plasma
<b><math>R</math></b>	: Radius of the fireball
<b><math>R_C</math></b>	: Canonical radius
<b>RHIC</b>	: Relativistic Heavy-Ion Collider
<b>S</b>	: Strangeness quantum number
<b>SHARE</b>	: Statistical Hadronization with Resonances
<b>STAR</b>	: Solenoidal Tracker at RHIC
<b>THERMUS</b>	: A Thermal Model Package for ROOT
<b><math>T_{ch}</math></b>	: Chemical freeze-out temperature
<b><math>\mu_B</math></b>	: Baryon chemical potential
<b><math>\mu_Q</math></b>	: Charge chemical potential
<b><math>\mu_S</math></b>	: Strangeness chemical potential
<b><math>\gamma_S</math></b>	: Strangeness saturation factor



## LIST OF TABLES

	<u>Page</u>
<b>Table 2.1</b> Four fundamental forces and gauge bosons [3]. .....	4
<b>Table 2.2</b> Classification of particles by their spin [3]. .....	4
<b>Table 2.3</b> Properties of quarks [4]. .....	5
<b>Table 2.4</b> Properties of leptons [5]. .....	5



## LIST OF FIGURES

	<u>Page</u>
<b>Figure 2.1</b> : Space-time evolution of strongly interacting matter [7].	7
<b>Figure 2.2</b> : The comparison of STAR data (full circles) in pp collisions at $\sqrt{s} = 200$ GeV and THERMUS results (solid lines). The chemical freeze-out temperature is $T_{ch} = 171 \pm 9$ MeV. [13].	9
<b>Figure 2.3</b> : The comparison of STAR data (full circles) from AuAu collisions at $\sqrt{s_{NN}} = 200$ GeV and THERMUS results (short lines). The chemical freeze-out temperature is $T_{ch} = 168 \pm 6$ MeV [13].	10
<b>Figure 2.4</b> : The ALICE data in pp collisions at $\sqrt{s} = 0.9$ TeV together with the corresponding predictions performed by THERMUS [14].	11
<b>Figure 2.5</b> : The ALICE data in PbPb collisions at $\sqrt{s_{NN}} = 2.76$ TeV and the corresponding predictions with different temperature parameters; $T = 148$ MeV and $T = 164$ MeV [15].	12
<b>Figure 3.1</b> : The nucleon-nucleon center-of-mass energy dependency of strangeness suppression factor, $\gamma_s$ [42].	20
<b>Figure 4.1</b> : Comparison of the STAR data in pp collisions at $\sqrt{s} = 200$ GeV [62, 63] and the THERMUS results. The canonical ensemble fit parameter is $T_{ch} = 158 \pm 0.5$ MeV. The fixed parameters are $\gamma_s = 0.59$ and $R = 4$ fm.	28
<b>Figure 4.2</b> : Comparison of the STAR data in pp collisions at $\sqrt{s} = 200$ GeV [62] and the THERMUS results. The canonical ensemble fit parameter is $T_{ch} = 167 \pm 2.4$ MeV. The fixed parameters are $\gamma_s = 0.5$ and $R = 4.1$ fm.	29
<b>Figure 4.3</b> : Comparison of the STAR data in pp collisions at $\sqrt{s} = 200$ GeV [63] and the THERMUS results. The canonical ensemble fit parameter is $T_{ch} = 157 \pm 0.6$ MeV. The fixed parameters are $\gamma_s = 0.6$ and $R = 3.85$ fm.	29
<b>Figure 4.4</b> : Comparison of the STAR data in dAu collisions at $\sqrt{s_{NN}} = 200$ GeV [62, 63] and the THERMUS results. The strangeness canonical ensemble fit parameters are $T_{ch} = 166 \pm 3.8$ MeV, $\mu_B = 5 \pm 1.9$ MeV and $\mu_Q = 18.3 \pm 3.3$ MeV and the fixed parameters are $\gamma_s = 0.68$ , $R_C = 3$ fm and $R = 7$ fm.	30
<b>Figure 4.5</b> : Comparison of the STAR data in dAu collisions at $\sqrt{s_{NN}} = 200$ GeV [62, 63] and the THERMUS results. The grand canonical ensemble fit parameters are $T_{ch} = 165 \pm 4$ MeV, $\mu_B = 2 \pm 1$ MeV, $\mu_S = 2 \pm 1$ MeV and $\mu_Q = 15 \pm 3$ MeV while the fixed parameters are $\gamma_s = 0.66$ and $R = 7$ fm.	30

- Figure 4.6** : Comparison of the STAR data in dAu collisions at  $\sqrt{s_{NN}} = 200$  GeV [62] and the THERMUS results. The strangeness canonical ensemble fit parameters are  $T_{ch} = 180 \pm 5.6$  MeV,  $\mu_B = 14.8 \pm 6$  MeV and  $\mu_Q = 1 \pm 0.35$  MeV. The fixed-type parameters are  $\gamma_S = 0.65$ ,  $R_C = 3.3$  fm and  $R = 7$  fm. .... 31
- Figure 4.7** : Comparison of the STAR data in dAu collisions at  $\sqrt{s_{NN}} = 200$  GeV [62] and the THERMUS results. The grand canonical ensemble fit parameters are  $T_{ch} = 177 \pm 6$  MeV,  $\mu_B = 15 \pm 6$  MeV,  $\mu_S = 1.7 \pm 0.5$  MeV,  $\mu_Q = 1.2 \pm 0.5$  MeV. The fixed-type parameters are  $\gamma_S = 0.65$  and  $R = 7$  fm. .... 31
- Figure 4.8** : Comparison of the STAR data in dAu collisions at  $\sqrt{s_{NN}} = 200$  GeV [63] and the THERMUS results. The strangeness canonical ensemble fit parameters are  $T_{ch} = 163 \pm 10$  MeV,  $\mu_B = 40 \pm 6$  MeV,  $\mu_Q = 53.2 \pm 9$  MeV. The fixed parameters are  $\gamma_S = 0.7$ ,  $R_C = 2.3$  fm,  $R = 7$  fm. .... 32
- Figure 4.9** : Comparison of the STAR data in AuAu collisions at  $\sqrt{s_{NN}} = 200$  GeV [13] and the THERMUS results. The grand canonical ensemble fit parameters are  $T_{ch} = 200 \pm 1.4$  MeV,  $\mu_B = 42.5 \pm 1.2$  MeV,  $\mu_S = 11.6 \pm 2.7$  MeV and  $\mu_Q = -4 \pm 0.7$  MeV. The fixed parameters are  $\gamma_S = 0.96$  and  $R = 9$  fm. .... 33
- Figure 4.10**: Comparison of the STAR data in AuAu collisions at  $\sqrt{s_{NN}} = 200$  GeV [13] and the THERMUS results. The grand canonical ensemble fit parameters are  $T_{ch} = 200 \pm 1.7$  MeV,  $\mu_B = 51.6 \pm 7$  MeV,  $\mu_S = 14.8 \pm 4.3$  MeV,  $\mu_Q = 4.9 \pm 2.3$  MeV. The fixed parameters are  $\gamma_S = 1.5$  and  $R = 9$  fm. .... 33
- Figure 4.11**: Comparison of the STAR data in AuAu collisions at  $\sqrt{s_{NN}} = 200$  GeV [62] and the THERMUS results. The grand canonical ensemble fit parameters are  $T_{ch} = 173 \pm 5.8$  MeV,  $\mu_B = 22 \pm 4.6$  MeV,  $\mu_S = 2 \pm 0.6$  MeV and  $\mu_Q = 1 \pm 1.4$  MeV. The fixed parameters  $\gamma_S = 0.8$ ,  $R = 9$  fm. .... 34
- Figure 4.12**: T- $\mu_B$  dependency plot under the condition of  $\bar{p}/p = 0.769 \pm 0.055$  ratio taken from the STAR data [13]. The grand canonical ensemble fixed parameters are  $\mu_S = 10$  MeV,  $\mu_Q = -5.2$  MeV,  $\gamma_S = 0.86$  and  $R = 9$  fm. The solid line represents the fit function  $T = 7.4\mu_B - 38.74$ . .... 35
- Figure 4.13**: T- $\mu_S$  dependency plot under the condition of  $\bar{p}/p = 0.769 \pm 0.055$  ratio taken from the STAR data [13]. The grand canonical ensemble fixed parameters:  $\mu_B = 28.8$  MeV,  $\mu_Q = -5.2$  MeV,  $\gamma_S = 0.86$  and  $R = 9$  fm. The solid line represents the fit function  $T = 0.00068\mu_S^2 - 0.394\mu_S + 177.38$ . .... 35
- Figure 4.14**: T- $\mu_Q$  dependency plot under the condition of  $\bar{p}/p = 0.769 \pm 0.055$  ratio taken from the STAR data [13]. The grand canonical ensemble fixed parameters:  $\mu_B = 28.8$  MeV,  $\mu_S = 10$  MeV,  $\gamma_S = 0.86$  and  $R = 9$  fm. The solid line represents the fit function  $T = 7.7\mu_Q + 214.3$ . .... 36

- Figure 4.15:** T- $\gamma_S$  dependency plot under the condition of  $\bar{p}/p = 0.769 \pm 0.055$  ratio taken from the STAR data [13]. The grand canonical ensemble fixed parameters:  $\mu_B = 28.8$  MeV,  $\mu_S = 10$  MeV,  $\mu_Q = -5.2$  MeV and  $R = 9$  fm. The solid line represents the fit function  $T = -3.46\gamma_S + 177.2$ . ..... 36
- Figure 4.16:** T-R dependency plot under the condition of  $\bar{p}/p = 0.769 \pm 0.055$  ratio taken from the STAR data [13]. The grand canonical ensemble fixed parameters:  $\mu_B = 28.8$  MeV,  $\mu_S = 10$  MeV,  $\mu_Q = -5.2$  MeV and  $\gamma_S = 0.86$ . The solid line represents the fit function  $T = 174.28$ . ..... 37
- Figure 4.17:** Comparison of the ALICE data in pp collisions at  $\sqrt{s} = 900$  GeV [65] and the THERMUS prediction. The canonical ensemble fit parameter is  $T_{ch} \simeq 156$  MeV and the fixed parameters are  $\gamma_S = 0.6$  and  $R = 7.2$  fm. .... 38
- Figure 4.18:** Comparison of the ALICE data in pp collisions at  $\sqrt{s} = 900$  GeV [65] and the THERMUS results. The strangeness canonical ensemble fit parameters are  $T_{ch} = 146 \pm 4$  MeV,  $\mu_B = 2.9 \pm 1.2$  MeV and  $\mu_Q = 0.61 \pm 0.4$  MeV. The fixed parameters are  $\gamma_S = 0.67$ ,  $R_C = 4.3$  fm and  $R = 6.5$  fm. .... 38
- Figure 4.19:** Comparison of the ALICE data in PbPb collisions at  $\sqrt{s_{NN}} = 2.76$  TeV [67–69] and the THERMUS results. The grand canonical ensemble fit parameters are  $T_{ch} = 162 \pm 0.9$  MeV,  $\mu_B = 8.9 \pm 0.24$  MeV,  $\mu_S = 1 \pm 0.1$  MeV and  $\mu_Q = -5 \pm 0.43$  MeV. The fixed parameters are  $\gamma_S = 0.79$  and  $R = 10$  fm. .... 39
- Figure 4.20:** Comparison of the ALICE data in PbPb collisions at  $\sqrt{s_{NN}} = 2.76$  TeV [67–69] and the THERMUS results. The strangeness canonical ensemble fit parameters are  $T_{ch} = 163 \pm 0.5$  MeV,  $\mu_B = 9.5 \pm 0.9$  MeV and  $\mu_Q = -5 \pm 0.2$  MeV. The fixed parameters are  $\gamma_S = 0.8$ ,  $R_C = 6$  fm,  $R = 10$  fm. .... 39
- Figure 4.21:** T- $\mu_B$  dependency plot under the condition of  $\bar{p}/p = 0.9705 \pm 0.012$  taken from the ALICE data in PbPb collisions at  $\sqrt{s_{NN}} = 2.76$  TeV [66]. The grand canonical ensemble fixed parameters of  $\mu_S = 1$  MeV,  $\mu_Q = -2.8$  MeV,  $\gamma_S = 0.81$  and  $R = 10$  fm. The solid line represents the fit function  $T = 78.9\mu_B - 257.73$ . ..... 40
- Figure 4.22:** T- $\mu_Q$  dependency plot under the condition of  $\bar{p}/p = 0.9705 \pm 0.012$  taken from the ALICE data in PbPb collisions at  $\sqrt{s_{NN}} = 2.76$  TeV [66]. The grand canonical ensemble fixed parameters are  $\mu_B = 4$  MeV,  $\mu_S = 1$  MeV,  $\gamma_S = 0.81$  and  $R = 10$  fm. The solid line represents the fit function  $T = 72.46\mu_Q + 270.15$ . ..... 41
- Figure 4.23:** T- $\gamma_S$  dependency plot under the condition of  $\bar{p}/p = 0.9705 \pm 0.012$  taken from the ALICE data in PbPb collisions at  $\sqrt{s_{NN}} = 2.76$  TeV [66]. The grand canonical ensemble fixed parameters are  $\mu_B = 4$  MeV,  $\mu_S = 1$  MeV,  $\mu_Q = -2.8$  MeV and  $R = 10$  fm. The solid line represents the fit function  $T = 74.4$ . ..... 41

<b>Figure 4.24:</b>	T-R dependency plot under the condition of $\bar{p}/p = 0.9705 \pm 0.012$ taken from the ALICE data in PbPb collisions at $\sqrt{s_{NN}} = 2.76$ TeV [66]. The grand canonical ensemble fixed parameters are $\mu_B = 4$ MeV, $\mu_S = 1$ MeV, $\mu_Q = -2.8$ MeV, $\gamma_S = 0.81$ . The solid line represents the fit function $T = 74.38$ . .....	42
<b>Figure 5.1 :</b>	The center of mass energy dependency of baryon chemical potential. See text for details. ....	46
<b>Figure 5.2 :</b>	The center of mass energy dependency of chemical freeze-out temperature. See text for details. ....	46
<b>Figure 5.3 :</b>	The upper and the lower section showing the energy dependencies of T and $\mu_B$ in heavy-ion collisions, respectively [69]. ....	47
<b>Figure 5.4 :</b>	The extended version of the plot shown in Figure 5.3. The upper and the lower section again showing the energy dependencies of T and $\mu_B$ in heavy-ion collisions, respectively. ....	48

# STATISTICAL-THERMAL MODEL DESCRIPTION of HADRON YIELDS in HIGH ENERGY COLLISIONS

## SUMMARY

Statistical-thermal model has become remarkably successful for describing the particle production in relativistic heavy-ion collisions. Comparison of the experimental results and the theoretical predictions in a given energy range has provided the thermodynamic variables of strongly interacting matter at chemical freeze-out point. Eventually, this comparison has made the phase diagram of this strongly interacting matter possible to be understood. To this extent, the identification of chemical freeze-out points of the collisions taking place in LHC at higher energies is vital for the completeness of the analysis of the statistical-thermal approach.

The statistical-thermal method is an instrument used in the quantitative analysis of the phase diagram of hadronic matter and the studies performed for relativistic heavy-ion collisions have compatible results with the experimental data. The basic principle in this approach is the medium created in the collisions is supposed to be in thermal equilibrium. It is assumed that the hadron species to be produced in the medium do not change at the chemical-freeze out point. When the particle yields/ratios in the medium becomes constant, it enables the particles created in the collisions to carry out information about the thermal condition of the medium at chemical-freeze out point.

In the light of the success of this approach, A Thermal Model Package for ROOT (THERMUS), has been developed by performing some calculations within three distinct formalisms. It is possible to make calculations with canonical, grand canonical and strangeness (mixed) canonical ensembles using the analysis tools.

In this study, the particle production in proton-proton (pp), Deuterium-Gold (dAu) and Gold-Gold (AuAu) collisions in Relativistic Heavy-Ion Collider (RHIC) and proton-proton (pp), Lead-Lead (PbPb) collisions in LHC have been reproduced in the context of the THERMUS analysis. While the particle yields/ratios have been produced, the relevant statistical-thermal parameters were extracted using THERMUS. These parameters are called the chemical freeze-out point parameters by the statistical-thermal approach.

In the analysis, the strangeness canonical ensemble used in the predictions has been emphasized widely in this thesis as the success of the approach. Also, the temperature dependency of other statistical-thermal parameters specified by THERMUS has been included to the extent of this study. Finally, the center of mass energy dependencies of the chemical freeze-out temperature and baryon chemical potential extracted from the analysis throughout the thesis have been given as the ultimate goal of the whole study.



# YÜKSEK ENERJİLİ ÇARPIŞMALARDA OLUŞAN ÜRÜN MİKTARLARININ İSTATİSTİKSEL TERMAL MODEL YÖNTEMİYLE İNCELENMESİ

## ÖZET

Bilim insanlarının büyük bir kısmı, bugün evrende gördüğümüz maddenin orjinini günümüzden 15 milyar yıl önce Büyük Patlama'nın oluşmasıyla açıklamaktadırlar. Büyük Patlama'dan birkaç mikrosaniye sonra oluşan ortamın; serbest halde bulunan ve günümüz bilgisiyle maddeyi oluşturan en küçük yapıtaşları olan kuark ve gluonlardan oluştuğu düşünülmektedir. Kuark-Gluon Plazma (QGP) adını alan maddenin bu hali; evrenin genişleyip soğumasıyla birlikte bir faz geçişine uğrayıp hadron ismini alan yapıların içerisine hapsolür. Yaygın olarak bilinen ve evreni oluşturan en temel hadronlar proton ve nötronlardır.

Hadronların içerisine hapsolmüş halde bulunan kuark ve gluonların laboratuvar ortamında serbest hale geçip Büyük Patlama'nın yeniden oluşması için aşırı yüksek sıcaklık ve yoğunluk gibi şartlar söz konusudur. Modern bilim ve mühendislik gelişmeleri ışığında bu şartlar sağlanarak; QGP ortamının günümüzde oluşturulması mümkün olmuştur. Bu çalışmaların evrenin oluştuğu ilk zamanlara ayna tutup maddenin oluşumunu açıklaması beklenmektedir.

Avrupa Nükleer Araştırma Merkezi (CERN) dünyanın dört bir yanından gelen bilim insanlarının evreni oluşturan maddenin temel yapısını anlamaya yönelik uğraşlarına ev sahipliği yapmaktadır. Bu yapıtaşlarını keşfeden, niteliklerini ve etkileşimlerini inceleyen dünyanın en gelişkin cihazları bu merkezde bulunmaktadır.

Büyük Hadron Çarpıştırıcısı (LHC), CERN'de bulunmakta olup dünyanın en güçlü parçacık çarpıştırıcısıdır. LHC, dairesel bir parçacık hızlandırıcısı olup süperiletken mıknatıslardan oluşur ve 27 kilometre uzunluğundadır. LHC'deki 1232 dipol mıknatıs parçacık demetlerini dairesel yörüngeye uygun şekilde bükme için kullanılırken, 392 kuadropol mıknatıs ise demetlerin odaklanmasında görevlidir. Parçacıkların ivmelenmesi için kullanılan bileşenler LHC'de koşturulan demetteki parçacıkların ışık hızına çok yakın hızlara erişmesini sağlamaktadırlar. Karşılıklı iki parçacık demeti hızlandırıldığında çok yüksek enerjilerde çarpışmalar gerçekleşmektedir. LHC'de elde edilen en yüksek enerji 8 TeV olup bu enerjinin yakın zamanda 15 TeV'e kadar yükseltilmesi beklenmektedir.

LHC'nin fizik programına dahil edilen deneylerden biri de Büyük İyon Çarpıştırıcısı Deneyi (ALICE)'dir. ALICE, yüksek enerjilerde gerçekleşen ağır iyon çarpışmalarında güçlü kuvvet ile etkileşen maddenin özelliklerini inceleyen bir deneydir. ALICE'deki bilim insanlarının sürdürdükleri araştırmalar QGP oluşumuna ışık tutmaktadır.

Teorik alanda yapılan çalışmalar ALICE ve benzeri deneylerde elde edilen verilerin

değerlendirilmesi ve doğrulanması için başvurulması gereken tamamlayıcı öğelerdir. Bu nedenle geliştirilen teorik temelli istatistiksel-termal yaklaşım; yüksek enerjili ağır iyon çarpışmalarında elde edilen QGP oluşumunu inceler.

Bu yaklaşımın dayandığı temelin anlaşılması için deneylerde oluşan fiziksel süreçlere değinilmelidir. Yüksek enerjili iki parçacık demetinin çarpıştırılmasıyla birlikte hadronların içerisine hapsolmuş güçlü kuvvetle etkileşen partonlar -kuark ve gluonlar- serbest hale geçer. Bu olayın hemen arkasından termal dengenin sağlanmasıyla beraber QGP oluşumu beklenir. Hızla soğuyan ve genişleyen ortamdaki bileşenler tekrar hadronların içerisine hapsolurlar ve sistem kimyasal donma noktası denilen noktaya eriştiğinde ortamdaki hadronların miktarları ve/veya birbirine olan oranları sabit kalır. Kimyasal donma noktasına erişildiğinde ortamdaki parçacık miktarları ve/veya oranlarının sabit kalmasının önemi; parçacıklar bu noktadan sonra detektör sistemleri tarafından tespit edilebilecek hale gelirler. Ayrıca çarpışmalar sonucu oluşan ortamın termodinamik değişkenleri belirlendiğinde ortam hakkında bilgi sahibi olunabilir.

Bu termodinamik değişkenler ile birlikte çarpışmalarda oluşan ürün miktarlarının belirlenmesinde kullanılan istatistiksel-termal yaklaşım, rölativistik ağır iyon çarpışmalarında deneysel olarak ölçülen parçacık miktarlarının tahmininde isabetli olmuştur. Böylelikle, bu çarpışmalardan elde edilen deneysel ölçümlerin teorik bir yaklaşım olan istatistiksel-termal model sonuçları ile karşılaştırılması; güçlü kuvvet ile etkileşen maddenin kimyasal donma noktasında elde edilen termodinamik parametrelerinin saptanması mümkün olmuştur ve asıl amaç olan faz diyagramının anlaşılabilmesini sağlamıştır. Bu bağlamda, kimyasal donma noktasındaki sıcaklık ve baryon kimyasal potansiyel gibi ortamın özelliklerini yansıtan iki başat parametrenin bulunması kritik bir noktadır. Bu yaklaşım çerçevesinde yürütülen çalışmaların bütünlüğü açısından LHC'de elde edilen yüksek enerjili ağır iyon çarpışmaları için de tespit edilmeleri gerekmektedir.

Hadronik maddenin faz diyagramının nicel analizi için kullanılan bu yaklaşımdaki temel kabul; çarpışma sonucu oluşan ortamın hadronlardan oluşan termal dengedeki bir ideal gaz olmasıdır. Söz konusu bu hadron gazı için yazılan bölüşüm fonksiyonu kullanılarak sıcaklık, hacim, entropi, birincil ve ikincil ürün parçacık miktarları gibi termodinamik değişkenler hesaplanabilir. Bu bölüşüm fonksiyonunun şeklini kullanılan istatistiksel topluluk belirlemektedir.

Bu yaklaşım ile yapılan analizlerde kimyasal donma noktası parametrelerinin öngörülen değerler ile örtüşmesi ve parçacık üretim miktarlarını isabetli bir şekilde tahmin edilebilmesi, THERMUS (A Thermal Model Package for ROOT) isimli analiz paketinin yazılmasına olanak sağlamıştır. THERMUS, ROOT uygulamalarına yönelik C++ programlama dili kullanarak yazılmış bir pakettir. İstatistiksel-termal modeli temel olarak yapılan hesaplamalar sonucu THERMUS, 3 farklı istatistiksel topluluk ile işlem yapabilmektedir. Bu topluluklar; büyük kanonik topluluk, kanonik topluluk ve acayip (karışık) kanonik topluluk olup; çarpışma sonucu oluşan parçacık miktarlarını her bir topluluk için farklı yaklaşım kullanarak tanımlar.

Büyük kanonik topluluk; ağır iyon çarpışmalarında en çok kullanılan topluluk olup bol miktarda ürün parçacık elde edilen Döteryum-Altın (dAu), Altın-Altın (AuAu) ve Kurşun-Kurşun (PbPb) gibi çarpışma sistemleri için oldukça başarılı sonuçlar

ortaya koymuştur. Bu toplulukta, B (baryon), S (acayıklık) ve Q (yük) gibi kuantum sayılarını taşıyan parçacıkların miktarı ile ilgili kimyasal potansiyeller ilgili parçacıkların üretimini kontrol üzere devreye girer. Kimyasal potansiyellerin varlığı ilgili kuantum sayılarını taşıyan parçacıkların miktarlarının ortalama değerler etrafında dalgalanmasına olanak tanır ve yine bu kimyasal potansiyeller aracılığıyla sisteme korunum yasaları uygulanır.

Kanonik topluluk ise proton-proton (pp) çarpışmalarının gerçekleştiği sistemlerde ağır iyon çarpışmalarına kıyasla az miktarda ürün oluşumu sebebiyle B,S ve Q gibi kuantum sayılarını taşıyan parçacıkların sayılarının tam olarak korunduğu topluluk türüdür. Bu toplulukta söz konusu parçacıkların miktarlarında dalgalanmaya izin yoktur ve kuantum sayıları üzerinde korunum yasaları uygulanır.

Son olarak, acayıp (karışık) kanonik toplulukta B ve Q kuantum sayılarını taşıyan parçacıklar için büyük kanonik topluluktaki prensip geçerliyken, S kuantum sayısına sahip parçacık miktarları için kanonik toplulukta olduğu gibi tam korunum kanunları esastır. Bu topluluk tüm çarpışma sistemleri için kullanılabilir ancak esas itibarıyla yüksek enerjilerdeki pp çarpışmaları için oldukça başarılı sonuçlar verdiğinin altı çizilmelidir.

Bu tez çalışmasında; öncelikli olarak RHIC (Rölativistik Ağır İyon Çarpıştırıcısı) fizik programında yer alan STAR (Solenoidal Tracker at RHIC) deneyi 200 GeV enerjili pp, dAu ve AuAu çarpışmalarına ait ölçümler istatistiksel-termal yaklaşımı çerçevesinde analiz edilmiştir. STAR detektörü, ALICE deneyinde sürdürülen çalışmalara benzer şekilde QGP oluşumunu incelemek için tasarlanmıştır. STAR deneyinden elde edilen veriler THERMUS analiz paketi aracılığıyla yeniden üretilmiştir ve bu tahmini sonuçları veren termodinamik parametreler QGP'nin oluştuğu ortamı yansıtması itibarıyla kimyasal donma noktası parametreleri olarak belirlenmiştir. Bu öncü çalışma, ALICE deneyinden elde edilen verilerin benzer şekilde analizinin yapılması ve yorumlanması için sağlıklı bir zemin hazırlamıştır. Benzer bir yol izlenerek 900 GeV enerjili pp çarpışmaları ile 2.76 TeV enerjili PbPb çarpışmaları için ALICE deney sonuçları; THERMUS paketi kullanılarak yeniden üretilmiştir. Analizlerde tespit edilmesi hedeflenen en önemli iki temel parametre; ortamın sıcaklığı ve baryon kimyasal potansiyeldir. Dolayısıyla bu çalışmanın da nihai hedefi olarak; LHC enerjilerindeki çarpışmalarda oluşan ortamın sıcaklığı ve baryon kimyasal potansiyeli bulunmuştur.

Analizlerde; büyük kanonik topluluk, kanonik topluluk ve acayıp (karışık) kanonik topluluk olmak üzere yukarıda bahsi geçen her 3 istatistiksel topluluk için yapılan hesaplamalara yer verilmiştir. Bunun yanı sıra; daha önce çalışılmayan acayıp kanonik topluluğa sonuçların da başarılı olması sebebiyle geniş yer verilmiştir. Bu tezde yapılan çalışmaların en sağlıklı parametreleri vermesi amacıyla belirli bir deney seti için birden fazla istatistiksel topluluk kullanılarak analizler tekrar edilmiştir.

Çarpışma sonrasında oluşan aşırı yüksek sıcaklık ve yoğunluk şartları altındaki ortam düşünüldüğünde, diğer tüm parametrelerin sıcaklığa bağlı davranışının büyük önem taşıdığı düşünülmektedir. Bu düşünceden hareketle; istatistiksel-termal yaklaşım temel alınarak yapılan hesaplamalarda parametre olarak kullanılan bazı termodinamik değişkenlerin, sıcaklığa bağlı değişimi bu tez çalışması kapsamında gerçekleştirilmiştir.

Son olarak, tüm bu analizlerde elde edilen kimyasal donma noktası sıcaklığının ve baryon kimyasal potansiyelin enerjiye olan bağımlılığı verilmiştir. Bu anlamda, bu tez çalışmasındaki analizlerde elde edilen söz konusu değerlerin önceki çalışmalar ile tutarlılığı ilgili referanslar örnek gösterilerek ortaya konulmuştur.

## 1. INTRODUCTION

A majority of the physicists believe that the matter in the Universe today was created during the Big Bang nearly 15 billion years ago.

It is thought that the medium formed in a few microseconds after the Big Bang was filled up with free quarks and gluons which are, with today's knowledge, the tiniest constituents of matter. As the universe expanded and cooled, the quark-gluon plasma (QGP), the state of matter in these particular circumstances, experienced a phase transition and the quarks and gluons were eventually confined into hadrons. The well-known hadrons are the protons and neutrons that shape our universe today [1].

Quarks and gluons are normally confined in the hadrons and there are some technical requirements depending on extremely high temperature and density to make them liberate in the laboratory. However, in the light of modern science and engineering developments, QGP is created in the laboratory systems.

At CERN, the European Organization for Nuclear Research, scientists from all over the world are endeavoring to unravel the fundamental structure of matter. To this extent, the attempt to probe the building blocks of matter is governed by the world's most prominent instruments at this facility.

The Large Hadron Collider (LHC) located at CERN is the most powerful particle accelerator in the world that consists of a number of superconducting magnets along the 27-kilometre ring. 1232 dipole magnets is used to bend the beams while 392 quadrupole magnets focus the beams. The accelerator components of LHC are boosting the particles energy so that the particle beams travel at almost with the speed of light. Once the two opposite beams accelerate, they are collided at very high energies. The very recent center of mass energy reached at LHC is 8 TeV and this energy will be gradually increased up to 15 TeV.

A Large Ion Collider Experiment (ALICE) is one of the experiments performed in

the context of LHC physics program. It is devoted to explore the properties of strongly interacting matter created in heavy-ion collisions at LHC at high energies. The analysis being conducted in ALICE Collaboration provides insights into the properties of QGP. Complementary element of the experimental researches is the theoretical framework. It verifies the data measured from the collisions and it also evaluates the experimental data in physical aspect. Thus, the statistical-thermal approach is an effective tool to assign the thermo-dynamical quantities of the constituents of the medium created in the collisions. The statistical-thermal method has successfully reproduced the previous experiment results and has prediction capability for the future experiments at higher energies [2].

The objective of this thesis is to give the description of the baryon chemical potential and the temperature of the medium created in high energy collisions using statistical-thermal method. The predictions of the statistical-thermal approach reflecting the medium properties have been comprehensively studied in the way which describes the experimental data very well. In this work, the studies have been initiated by the reproduction of experimental measurements taken from the STAR data at RHIC energies and the parameters that qualify the medium associated with QGP formation have been identified. The analysis has been continued with the ALICE data at LHC energies and chemical freeze-out parameters have been defined as well. Finally, the center of mass energy dependencies of chemical freeze-out temperature and baryon chemical potential have been presented.

## 2. THE STANDARD MODEL OF PARTICLE PHYSICS

The Standard Model of particle physics encapsulates the precise understanding of the relation between elementary particles and the fundamental forces. The matter in the universe is explained to be made from elementary particles interacting by four fundamental forces.

The force acting on the constituents that form the matter is the strong force which has a short range around a diameter of a medium sized nucleus ( $\sim 10^{-15}$  m). The exchange particle attributed to strong force is "gluon" which carries the color charge of the strong interaction. There are eight independent types of gluon in Quantum Chromodynamics (QCD).

The weak force is responsible for both the radioactive decay and nuclear fusion of subatomic particles. The carriers of this force are " $W^\pm$  and Z bosons". The weak interaction has also a short range around  $10^{-16}$ - $10^{-17}$  m.

Electromagnetic force acts between electrically charged particles and also acts on physical processes associated with magnetic field. It has an infinite range and the "photon" is responsible for these interactions.

Another fundamental force is gravity which is an attractive force and has an infinite range like electromagnetism. Also, it acts on all particles having mass and it is expected to interact via the -not yet found- "graviton".

In Table 2.1 [3], four fundamental forces are listed in order of decreasing strength. Here the word "strength" represents an ambiguous notion since it depends on how far one stands from the source and the nature of force.

In the Standard Model of particle physics, particles with half-integral spin are called fermions while those with integer spin are called boson. The classification of the elementary particles on the basis of their spin number is given in Table 2.2 [3]. The most important system is spin = 1/2; the proton, neutron, electron, all quarks and

**Table 2.1:** Four fundamental forces and gauge bosons [3].

Force	Strength	Theory	Mediator
Strong	10	Chromodynamics	Gluon
Electromagnetic	$10^{-2}$	Electrodynamics	Photon
Weak	$10^{-13}$	Flavordynamics	W and Z
Gravitational	$10^{-42}$	Geometrodynamics	Graviton

**Table 2.2:** Classification of particles by their spin [3].

Bosons (integer spin)		Fermions (1/2-integer spin)	
Spin 0	Spin 1	Spin 1/2	Spin 3/2
-	Mediators	Quarks, leptons	-
Pseudo-scalar mesons	Vector mesons	Baryon octet	Baryon decuplet

leptons carry spin 1/2. In Table 2.2, only the mediators (force carriers), quarks and leptons are all elementary particles while the others are composite particles.

There are three generations (or families) in Standard Model. Each generation is split into two leptons and two quarks. However, within these three generations, the generation itself does not change the interaction behaviour of particles.

There are six types of quarks defined as flavours: up (u), down (d) (first generation), strange (s), charm (c) (second generation), bottom (b), top (t) (third generation). Some properties of these quarks are listed in Table 2.3 [4]. The electric and baryonic charge attributed to quarks are fractional. Mesons and baryons, given in Table 2.2, which are also collectively called hadrons are made of these quarks.

Leptons are other type of fermions which undergo electromagnetic and/or weak interactions. The first family of leptons are  $e^-$  and  $\nu_e$ , the second family consists of  $\mu^-$  and  $\nu_\mu$  and the third generation of leptons are  $\tau^-$  and  $\nu_\tau$ . Some properties of leptons are listed in Table 2.4 [5].

The elementary bosons with spin 1 are the four gauge bosons; photon, gluon, Z and  $W^\pm$ . The other elementary boson is Higgs boson ( $H^0$ ) which was recently discovered at CERN. It is the particle with zero spin and it is thought that it helps to explain the origin of mass of subatomic particles. At the time Table 2.2 [3] was arranged, since the Higgs boson had not been discovered yet, it is not included to the table.

**Table 2.3:** Properties of quarks [4].

particle	mass [MeV/c <sup>2</sup> ]	electric charge	baryon number	spin
u	1.5-3.0	2/3	1/3	1/2
d	3-7	-1/3	1/3	1/2
s	95±25	-1/3	1/3	1/2
c	1.25±0.09x10 <sup>3</sup>	2/3	1/3	1/2
b	4.20±0.07 x10 <sup>3</sup>	-1/3	1/3	1/2
t	174±3.3x10 <sup>3</sup>	2/3	1/3	1/2

**Table 2.4:** Properties of leptons [5].

leptons	electric charge	mass
$e^-$	-e	0.511 MeV/c <sup>2</sup>
$\nu_e$	0	< 2 eV/c <sup>2</sup>
$\mu^-$	-e	106 MeV/c <sup>2</sup>
$\nu_\mu$	0	< 0.19 MeV/c <sup>2</sup>
$\tau^-$	-e	1.78 GeV/c <sup>2</sup>
$\nu_\tau$	0	< 18.2 MeV/c <sup>2</sup>

## 2.1 Quantum Chromodynamics

QCD is the theory of strong interaction describing the interactions between quarks and gluons which form the hadrons such as proton, neutron and pion. It is assumed that hadrons, strongly interacting particles, emerge as particle excitations in a quantum field theory of quarks and gluons as fundamental degrees of freedom.

The name of the theory, QCD, comes from color symmetry. The color hypothesis states that each quark comes in one of three colors red (r), green (g) or blue (b) while the corresponding anti-quarks are anti-colored:  $\bar{r}$ ,  $\bar{g}$  and  $\bar{b}$ . The hypothesis furthermore states that hadrons are color singlets ("white"). The quarks become distinguishable by labelling each with a different color.

In QCD, color plays the role of charge and gluons are the quanta of the color field which bind the quarks into hadrons. Unlike photons having zero electrical charge, the gluons themselves carry a color charge [6].

The up, down and strange quarks are known as very light quarks. In experiments, the searches for such light objects -states- having fractional electric charge have fallen through [4]. To be more precise, when the quarks confined into hadrons are separated, the force between quarks does not reduce meaning that the energy stems from this force is still enough to create a quark thus another quark pair. The fact that the quarks

are forever bound into hadrons is stated as confinement.

Under the strong interactions, quarks bind into hadrons which is classified as mesons ( $q\bar{q}$ ) and baryons ( $qqq$ ). However, it is expected that quarks and gluons become free in a strongly interacting medium at high enough temperatures and large enough densities [4].

## 2.2 Quark-Gluon Plasma

The evolution of hadronic matter into a state consists of various types of hadrons and the stage in the evolution of the early universe is quite similar. One of the aims of relativistic heavy-ion collisions is to obtain information about the basic physical processes which are expected to lead theoreticians to the point where the whole Universe hadronized [1].

In high energy collisions, hot and dense matter -so called fireball- exists for a very short time. After the fireball expanded and cooled, it is thought that the quark matter in the medium forms hadrons in Hadron Gas (HG) phase.

In Figure 2.1 [7], the phase diagram showing a four-phase structure of strongly interacting matter is presented. The four stages in the phase diagram occurred in ultra-relativistic nucleus-nucleus collisions can be briefly summarized as follows:

(i) In the "Pre-equilibrium" stage in Figure 2.1, the dominant mechanism is the parton-parton (quarks and gluons) scatterings in the region where the two nuclei collide. As a result, a huge amount of energy is deposited in the medium while the thermal equilibrium is not maintained yet. The duration of this state is expected to be about 1 fm/c.

(ii) In the second -Equilibrated QGP- stage, the QGP is expected to exist while the thermal equilibrium is obtained by the parton-parton interactions in the medium.

(iii) The volume of the system is continuing to expand and the hadronic matter is getting cooler. At a critical temperature,  $T_c$ , the confinement of quarks and gluons into hadrons occurs if the first order phase transition is supposed to exist in the "mixed phase". The time of this state is relatively longer ( $\tau > 10$  fm/c).

(iv) In HG phase, the hadron-hadron interactions in the medium sustain volume

expansion and this results in the decrease of the temperature of the system. The hadronic interactions cease after the medium attains a definite temperature and size. At this freeze-out stage, the multiplicity or particle ratios remain constant and hadrons can escape from the system so the particles can be detected. Here multiplicity is the number of particle yields created in the collisions per unit volume per event. Also, particle ratio is a ratio of particle yields of different species or antiparticle to particle yields of same species.

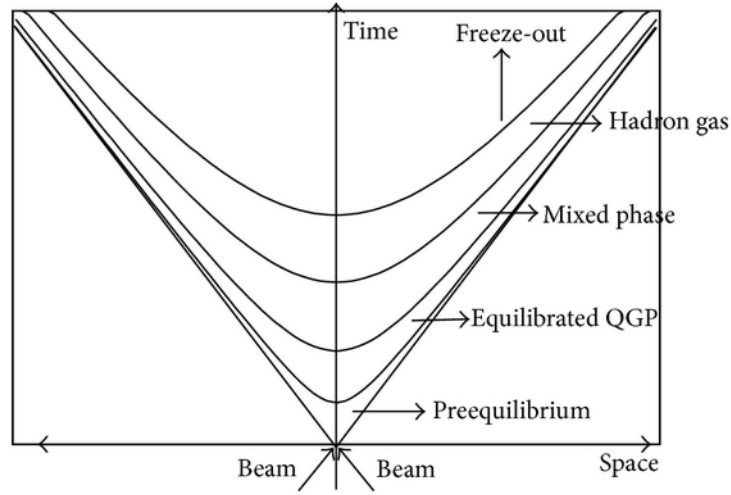


**Figure 2.1:** Space-time evolution of strongly interacting matter [7].

The freeze-out is classified as two stages; kinetic and thermal freeze-out. When the elements of the HG do not interact via inelastic collisions, this is called as chemical freeze-out and the elastic collisions in the fireball subsequently do not exist any more, this stage is described as thermal freeze-out [7, 8].

The QGP formation can not be directly understood without obtaining solid evidences since it occurs in a very brief time. Fortunately, there are several signals verifying the QGP existence [9]. In 1982, Rafelski and Muller suggested that the strange quark abundance in the hadronic medium is one of the signals of QGP formation [10]. The reactions causing the increase in the number of strange quarks are:

$$q\bar{q} \rightarrow s\bar{s} \quad (2.1)$$

$$gg \rightarrow s\bar{s} \quad (2.2)$$

Briefly, if there is an increase in the number of strange quarks observed in the medium occurring in the relativistic collisions, this is the consequence of the low energetic  $gg$  reactions since the dominant channel is the gluon channel [9].

## **2.3 Relativistic Collisions**

### **2.3.1 Proton-proton collisions**

The analysis of proton-proton (pp) collisions, at first stage, is the appropriate step to comprehend the nature of the heavy-ion collisions at relativistic energies. The data obtained from pp collisions is evaluated as reference for heavy-ion physics. Besides, as the same detector is used for both pp and heavy-ion collisions, the systematic uncertainties will be minimized in that way. The particle production in pp collisions is expected to be low and the system is small sized. As a utility, the detector calibration is thought to be easier [9].

Since QGP is expected to exist in proton-antiproton collisions at 1.8 TeV center of mass energies [11], it is not wrong to say that QGP formation is also possible in pp collisions at LHC.

### **2.3.2 Relativistic heavy-ion collisions**

The investigation of very early Universe naturally demands an infinite system size. The physical systems studied in the laboratories do not serve the infinite size since there are not any convenient volumes larger than Gold (Au) and Lead (Pb). However, the availability of particle production at high energies and the existence of fluctuation effects are unique tools to access various physical states. Eventually, the desired phase transition to observe QGP can be reached in relativistic heavy-ion collisions [1].

One of the arguments why collisions of relativistic heavy-ion is favorable for the QGP formation can be explained as follows: The medium created in these collisions is rich in strangeness enhancement and this abundance is not suppressed compared to pp collisions. Since the strangeness production is the signal of QGP formation, heavy-ion collisions carry valuable information regarding the nature of hadronic matter. Before the analysis to be performed in the frame of statistical-thermal approach, giving a

number of former analysis will make a contribution for the accuracy of this thesis study.

## 2.4 Previous Proton-Proton and Heavy-Ion Results

The previous studies of the comparison of experimental data taken from STAR and ALICE experiments are presented together with THERMUS predictions in order to emphasize the necessity of the comprehensive analysis.

### 2.4.1 Spectra of STAR experiment

The STAR detector primarily designed to study the formation of QGP created in relativistic heavy-ion collisions. It is one of the experiments at RHIC in Brookhaven National Laboratory. Hence, the STAR results are expected to be comparable with those of ALICE since both experiments search for the same phenomenon, the QGP.

The two plots, given in Figure 2.2 and 2.3, show the comparisons of STAR data in pp collisions at  $\sqrt{s} = 200$  GeV and AuAu collisions at  $\sqrt{s_{NN}} = 200$  GeV together with corresponding THERMUS predictions.

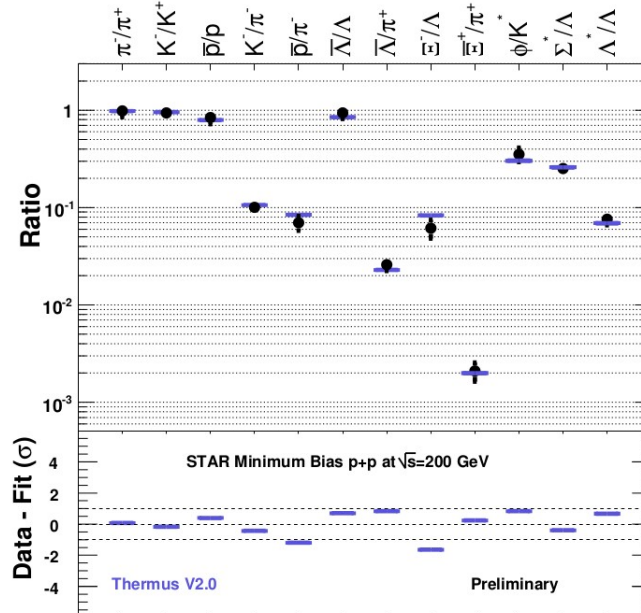


**Figure 2.2:** The comparison of STAR data (full circles) in pp collisions at  $\sqrt{s} = 200$  GeV and THERMUS results (solid lines). The chemical freeze-out temperature is  $T_{ch} = 171 \pm 9$  MeV. [13].

### 2.4.1.1 Proton-proton collisions

The experimental data obtained from pp collisions at STAR is compared with THERMUS V2.0 [12] predictions in Figure 2.2 [13]. The prediction is represented by solid lines whereas the STAR data is represented by full circles. At the bottom of the plot, the data-THERMUS results differences are also included. The chemical freeze-out temperature extracted by THERMUS is  $T_{ch} = 171 \pm 9$  MeV.

While the data consisting of non-resonance particles is reproduced quite well by THERMUS, the prediction for some resonances is not very good.

### 2.4.1.2 Gold-Gold collisions

The method similar to pp collisions is followed for Gold-Gold (AuAu) collisions to plot the comparison of the STAR data and THERMUS results. In Figure 2.3 [13], the STAR data AuAu collisions at  $\sqrt{s_{NN}} = 200$  GeV is compared to the THERMUS results. The chemical freeze-out temperature extracted by THERMUS for this collision system is  $T_{ch} = 168 \pm 6$  MeV. The full circles are again used for STAR data where the solid lines are for THERMUS prediction.

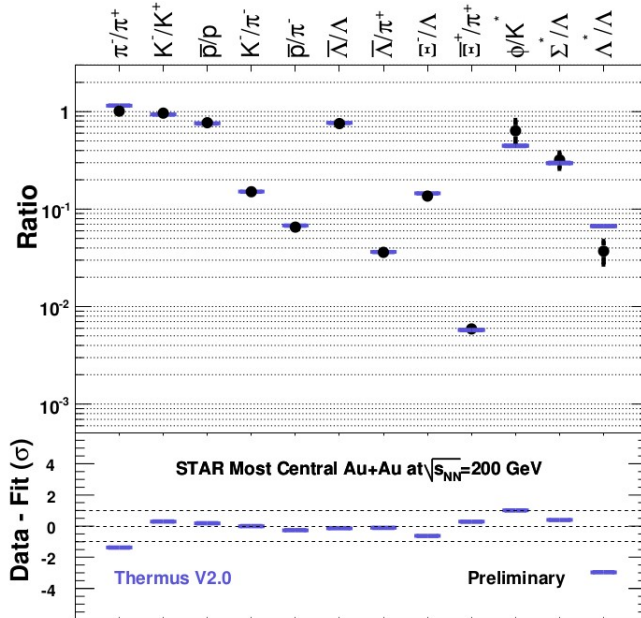


**Figure 2.3:** The comparison of STAR data (full circles) from AuAu collisions at  $\sqrt{s_{NN}} = 200$  GeV and THERMUS results (short lines). The chemical freeze-out temperature is  $T_{ch} = 168 \pm 6$  MeV [13].

The same fashion occurs in Figure 2.3 that the THERMUS prediction for STAR data consisting of non-resonance particles does not fit well with the corresponding experimental data.

## 2.5 Spectra of ALICE Experiment

The ALICE detector in LHC is also designed to engage the QGP formation and its physical processes. Since the analysis of ALICE data with THERMUS establishes the origin of this study, the insufficient description of experimental data should be particularly highlighted by giving a piece of work at a glance.

In the following, the previous results of the comparison of ALICE data in pp collisions at  $\sqrt{s} = 900$  GeV and PbPb collisions at  $\sqrt{s_{NN}} = 2.76$  TeV are represented with corresponding THERMUS predictions.

### 2.5.1 Proton-proton collisions

In Figure 2.4 [14], the ALICE data measured in pp collisions at  $\sqrt{s} = 0.9$  TeV and the THERMUS results are shown. Unfortunately, the chemical freeze-out temperature is not given in [14]. It is quite clear that the THERMUS prediction does not make good job for describing most of the experimental data, as a consequence, a detailed analysis achieved with experimental data and statistical-thermal method is required.

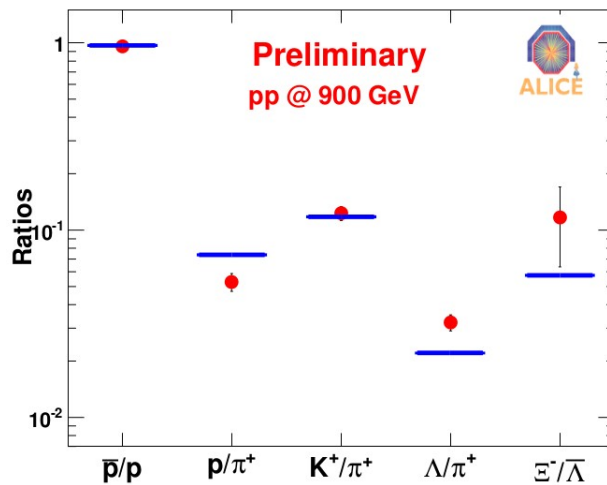


**Figure 2.4:** The ALICE data in pp collisions at  $\sqrt{s} = 0.9$  TeV together with the corresponding predictions performed by THERMUS [14].

## 2.5.2 Lead-Lead collisions

Since the medium formed in the collisions of relativistic heavy-ion is observed to comprise abundant number of strangeness content and it is the signature of QGP formation, it is thought that the phase transition to observe QGP must have also existed in Lead-Lead (PbPb) collision system.

Presenting a piece of work related to the statistical-thermal model analysis of PbPb collisions would be complementary and more detailed study would be necessary.

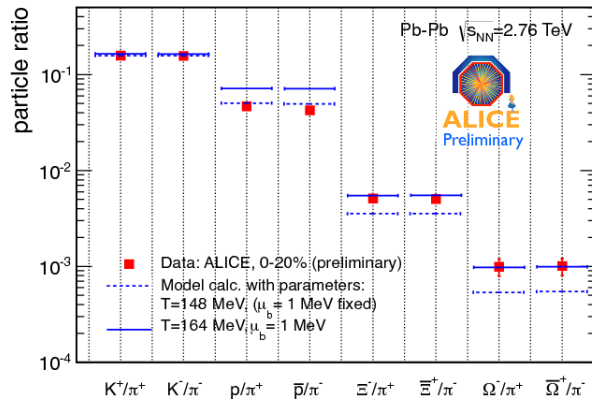


**Figure 2.5:** The ALICE data in PbPb collisions at  $\sqrt{s_{NN}} = 2.76$  TeV and the corresponding predictions with different temperature parameters;  $T = 148$  MeV and  $T = 164$  MeV [15].

In Figure 2.5 [15], the ALICE data taken from PbPb collisions at  $\sqrt{s_{NN}} = 2.76$  TeV is given with two distinct predictions which are obtained with the following temperature values:  $T = 148$  MeV and  $T = 164$  MeV.

### **3. THEORETICAL MODELS**

The comprehension and the interpretation of experimental data without theoretical approaches would be insufficient within a basic scientific frame. In the context of this aspect, those approaches will be shortly listed in the following. Also, a rather wide explanation of statistical-thermal approach which forms the theoretical background of the analysis achieved in this study will be presented.

Perturbative QCD (pQCD) basically aims to explain the structure of a system consists of multi-parton produced in QCD processes in a quantitative aspect in order to get information about confinement by comparing the quark-gluon formation properties with the final states where hadrons exist in hard processes [16]. In the soft processes where pQCD models are not applicable to the events, Dual Parton Model (DPM) is an adequate phenomenological treatment [17].

PHOJET [18] is a Monte Carlo event generator based on DPM for the soft processes and pQCD for hard interactions. Also, PYTHIA [19] is another QCD-based program which is used to generate events and it can distinguish 240 different physical processes.

In the next section, the main theoretical approach for QGP formation at high energy collisions is extensively introduced as baseline of this thesis study.

#### **3.1 Statistical-Thermal Model**

In 1948, Heinz Koppe purposed the notion of the applicability of statistical physics into elementary particle physics and investigated the particle production processes in the frame of statistical physics [20]. In 1964, Hagedorn used all tools of statistical physics and analysed the high energy phenomena leading to the solution of many-particle systems. The analysis of particle production in high energy collisions provides an evidence for the chemical equilibrium in the final state [21]. The particle production mechanism in the relativistic collisions performed in a wide range of

energies is successfully described by this approach [22–24]. The quantitative analysis of the phase diagram of strongly interacting matter is made possible by the help of statistical-thermal approach and this results in the determination of chemical freeze out temperature.

Statistical-thermal method assumes that the medium created after the collisions is an ideal gas which consists of hadrons [25]. At the freeze-out zone where all the hadrons reach to chemical and thermal equilibrium, the particle multiplicity and/or ratios do not alter. From low energy values to very high energies, the particle abundances measured in the experiments are studied in the assumption of chemical equilibrium. Thermodynamics quantities -such as entropy, energy, primary and secondary particle yields- can be obtained by the evaluation of hadron gas partition.

The partition function which describes the statistical properties of a system in thermodynamic equilibrium is formed depending on the statistical ensemble used for calculations. The following three ensembles can be used for statistical-thermal method applications.

### 3.1.1 The grand canonical ensemble

The grand canonical (GC) ensemble is the most used ensemble in the applications of relativistic collisions of heavy-ion [26–28]. The validity of GC approach is practicable when the particles carrying B (baryon), S (strangeness) and Q (charge) quantum numbers are abundant [29]. The chemical potentials specified for the given quantum numbers are introduced to allow fluctuations around conserved averages. The conservation laws are also applied through these chemical potentials.

Supposing the fireball treated as a gas composed of only one hadron species  $i$  having energy levels  $\{ \varepsilon_i^1, \varepsilon_i^2, \dots \}$ , the partition function for this gas,  $Z_i^{GC}$ , is written as follows and it can be used for computation of thermodynamic variables:

$$Z_i^{GC} = \prod_{states j} (1 \pm e^{-\beta(\varepsilon_i^j - \mu_i)})^{\pm 1} \quad (3.1)$$

Here,  $\mu_i$  is the chemical potential of species  $i$  and the reciprocal of temperature of the system,  $\beta$ , is given as  $\beta \equiv 1/T$ . The plus signs in the equation 3.1 refer to a gas composed of fermions and the minus signs are used for the bosons case.

In the large volume limits, the partition function turns into,

$$\ln Z_i^{GC}(T, V, \mu_i) = \frac{g_i V}{(2\pi)^3} \int d^3 p \ln (1 \pm e^{-\beta(E_i - \mu_i)})^{\pm 1} \quad (3.2)$$

where  $g_i$  is degeneracy of hadron species  $i$ ,  $V$  is the total volume of fireball and  $E_i = \sqrt{p^2 + m_i^2}$ , where  $m_i$  is the mass of particle.

If this given partition function is extended to a multi-constituents hadron gas having volume  $V$  and temperature  $T$ , the equation takes the following form:

$$\ln Z_i^{GC}(T, V, \{\mu_i\}) = \sum_{species} \frac{g_i V}{(2\pi)^3} \int d^3 p \ln (1 \pm e^{-\beta(E_i - \mu_i)})^{\pm 1} \quad (3.3)$$

In the relativistic collisions of heavy-ions, the particle numbers are not individually conserved, the quantum numbers  $B$ ,  $S$  and  $Q$  are conserved and  $\mu_i$  is given as follows:

$$\mu_i = B_i \mu_B + S_i \mu_S + Q_i \mu_Q \quad (3.4)$$

In the above equation,  $B_i$  is the baryon number,  $S_i$  is the strangeness and  $Q_i$  is the charge of hadron species  $i$  and the corresponding chemical potentials are;  $\mu_B$ ,  $\mu_S$ ,  $\mu_Q$  respectively.

The chemical potential  $\mu_B$  is a quantity which determines the energy required to add/remove a particle at fixed pressure, energy and entropy. By changing the baryon chemical potential, the difference in the number of baryons and anti-baryons present in the system can be regulated. However, densities of baryons and anti-baryons change together and absolute equilibrium is supposed while the relative chemical equilibrium controls the relative number of particles because of the value of the chemical potential.

One of the examples that highlights the role of baryon chemical potential is as the value of  $\mu_B$  approaches to zero, the density of the particles becomes identical to those of antiparticles meaning that the ratio of antiparticle to particle equals to 1. Thus, baryon chemical potential,  $\mu_B$ , is a measure of net baryon density. Also, it is one of the two significant parameters  $-T$  and  $\mu_B$  aimed to defined in the analysis since they give valuable information about QGP formation.

$\mu_S$  controls the difference between particles with strange and anti-strange quarks. It is expected that in a strangeness neutral system and at a fixed temperature, the value of

$\mu_S$  is always smaller than  $\mu_B$  because of the strangeness conservation [30]. Finally,  $\mu_Q$  is a parameter associated with charged particles controlling their densities.

All the thermodynamics variables can be obtained when the partition function is formed. Once the Grand Potential, the characteristic state function for the grand canonical ensemble,  $\Omega_{GC}(T, V, \{\mu_i\}) = E - TS - \sum_{\text{species } i} \mu_i N_i$  is introduced; the particle multiplicities, entropy, pressure and energy are calculated from the following differential forms:

$$N_i^{GC} = -\frac{\partial \Omega_{GC}}{\partial \mu_i}, \quad (3.5)$$

$$S^{GC} = -\frac{\partial \Omega_{GC}}{\partial T}, \quad (3.6)$$

$$P^{GC} = -\frac{\partial \Omega_{GC}}{\partial V}, \quad (3.7)$$

$$E^{GC} = T^2 \frac{\partial \ln Z^{GC}}{\partial T}. \quad (3.8)$$

### 3.1.2 The canonical ensemble

When statistical-thermal model is applied to the collisions of elementary particles [31, 32], a requirement arises for each quantum numbers to be treated canonically. Such a canonical description imposes the exact conservation of quantum numbers or particle numbers. To be more precise, in the collisions of elementary particle like pp systems having small volumes, the experimental particle production rate is small meaning that the system needs to be treated canonically. This treatment is necessary to fit the experimental data to the theoretical calculations.

Taking into account the case with a gas including multi-hadrons with both particles and anti-particles, the partition function is given by,

$$\begin{aligned} Z_{B,S,Q} &= \frac{Z_0}{(2\pi)^2} \int_{-\pi}^{\pi} d\phi_S \int_{-\pi}^{\pi} d\phi_Q \cos(S\phi_S + Q\phi_Q - B \arg \omega) \\ &\times \exp \left[ 2 \sum_{\text{mesons } j} z_j^1 \cos(S_j \phi_S + Q_j \phi_Q) \right] I_B(2|\omega|) \end{aligned} \quad (3.9)$$

where  $\omega \equiv \sum_{\text{baryons } j} z_j^1 e^{i(S_j \phi_S + Q_j \phi_Q)}$ ,  $z_j^1 \equiv \frac{g_j V}{(2\pi)^3} \int d^3 p e^{-\beta E_j}$  and  $Z_0$  represents the contribution of hadrons having no net charges while  $I_B(2|\omega|)$  is a function obtained using the following equation:  $I_n(z) = \frac{1}{2\pi} \int_{-\pi}^{\pi} e^{z \cos \theta} \cos n\theta d\theta$ .

The Helmholtz Free Energy is introduced as follows:

$$F \equiv E - TS = -T \ln Z_{B,S,Q} \quad (3.10)$$

Two variables below can be derived recalling the first law of thermodynamics ( $dE = TdS - PdV$ ):

$$S = -\frac{\partial F}{\partial T}, \quad (3.11)$$

$$P = -\frac{\partial F}{\partial V}. \quad (3.12)$$

Moreover, the multiplicity of hadron species  $i$ ,  $N_i^{B,S,Q}$ , is obtained by multiplying the single-partition function for particle  $i$  by a fictitious fugacity that controls the number of particle species  $i$  in the system,  $\lambda_i$ , differentiating with respect to  $\lambda_i$  and finally setting  $\lambda_i$  to 1:

$$N_i^{B,S,Q} = \left. \frac{\partial \ln Z_{B,S,Q}(\lambda_i)}{\partial \lambda_i} \right|_{\lambda_i=1} \quad (3.13)$$

$$\begin{aligned} N_i^{B,S,Q} &= \left( \frac{Z_{B-B_i, S-S_i, Q-Q_i}}{Z_{B,S,Q}} \right) \frac{g_i V}{(2\pi)^3} \int d^3 p e^{-\beta E_i} \\ &= \left( \frac{Z_{B-B_i, S-S_i, Q-Q_i}}{Z_{B,S,Q}} \right) N_i^{GC} |_{\mu_i=0} \end{aligned} \quad (3.14)$$

$$\begin{aligned} S^{B,S,Q} &= \frac{\partial (T \ln Z_{B,S,Q})}{\partial T} \\ &= \ln Z_{B,S,Q} + \sum_{\text{species } i} \left( \frac{Z_{B-B_i, S-S_i, Q-Q_i}}{Z_{B,S,Q}} \right) \frac{E_i^{GC} |_{\mu_i=0}}{T} \end{aligned} \quad (3.15)$$

$$\begin{aligned} P^{B,S,Q} &= \frac{\partial (T \ln Z_{B,S,Q})}{\partial V} \\ &= \sum_{\text{species } i} \left( \frac{Z_{B-B_i, S-S_i, Q-Q_i}}{Z_{B,S,Q}} \right) \frac{N_i^{GC} |_{\mu_i=0} T}{V} \\ &= \sum_{\text{species } i} \left( \frac{Z_{B-B_i, S-S_i, Q-Q_i}}{Z_{B,S,Q}} \right) P_i^{GC} |_{\mu_i=0} \end{aligned} \quad (3.16)$$

$$\begin{aligned}
E^{B,S,Q} &= F + TS^{B,S,Q} \\
&= \sum_{\text{species } i} \left( \frac{Z_{B-B_i, S-S_i, Q-Q_i}}{Z_{B,S,Q}} \right) E_i^{GC} \Big|_{\mu_i=0}
\end{aligned} \tag{3.17}$$

### 3.1.3 The strangeness canonical ensemble

In systems with smaller volumes or lower temperatures, a canonical description causes to a suppression of hadrons with non-zero quantum numbers. Also, the abundant number of baryons and particles with net charge are produced in the collisions of heavy-ion so the system can be treated grand-canonically. However, at the low temperature values obtained in the collisions, the poor production of strange particles demands to be treated strangeness as canonically. Taking into account these cases, the strangeness canonical ensemble is put forward to the application of statistical-thermal approach.

Within this ensemble, the strangeness is exactly fixed by its initial value of  $S$  in the system, for the baryon and charge contents of the system, the grand canonical ensemble treatment is valid.

For a hadron gas having strangeness  $S$  and obeying Boltzmann statistics, the partition function can be written as follows:

$$\begin{aligned}
Z_{B,S,Q} &= \frac{1}{2\pi} \int_{-\pi}^{\pi} d\phi_S e^{-iS\phi_S} \\
&\times \exp \left[ \sum_{\text{hadrons } i} \frac{g_i V}{(2\pi)^3} \int d^3 p e^{-\beta(E_i - \mu_i)} e^{iS_i \phi_S} \right]
\end{aligned} \tag{3.18}$$

In the equation 3.18, the summation is taken over both particles and anti-particles. Also  $\mu_i$  is given below:

$$\mu_i = B_i \mu_B + Q_i \mu_Q \tag{3.19}$$

The following thermodynamics quantities can also be calculated:

$$\begin{aligned}
N_i^S &= \left. \frac{\partial \ln Z_S(\lambda_i)}{\partial \lambda_i} \right|_{\lambda_i=1} \\
&= \left( \frac{Z_{S-S_i}}{Z_S} \right) \frac{g_i V}{(2\pi)^3} \int d^3 p e^{-\beta(E_i - B_i \mu_B - Q_i \mu_Q)} \\
&= \left( \frac{Z_{S-S_i}}{Z_S} \right) N_i^{GC} \Big|_{\mu_S=0}
\end{aligned} \tag{3.20}$$

$$\begin{aligned}
S^S &= \frac{\partial(T \ln Z_S)}{\partial T} \\
&= \ln Z_S + \sum_{\text{species } i} \left( \frac{Z_{S-S_i}}{Z_S} \right) \left( \frac{E_i^{GC}|_{\mu_S=0} - \mu_i N_i^{GC}|_{\mu_S=0}}{T} \right)
\end{aligned} \tag{3.21}$$

$$\begin{aligned}
P^S &= \frac{\partial(T \ln Z_S)}{\partial V} \\
&= \sum_{\text{species } i} \left( \frac{Z_{S-S_i}}{Z_S} \right) \left( \frac{N_i^{GC}|_{\mu_S=0} T}{V} \right) \\
&= \sum_{\text{species } i} \left( \frac{Z_{S-S_i}}{Z_S} \right) P_i^{GC}|_{\mu_S=0}
\end{aligned} \tag{3.22}$$

$$\begin{aligned}
E^S &= \Omega_{SCan} + TS^S + \sum_{\text{species } i} \mu_i N_i^S \\
&= \sum_{\text{species } i} \left( \frac{Z_{S-S_i}}{Z_S} \right) E_i^{GC}|_{\mu_S=0}
\end{aligned} \tag{3.23}$$

Here  $\Omega_{SCan}$  is Grand Potential defined for strangeness canonical ensemble and is given as follows:  $\Omega_{SCan}(T, V, \{\mu_i\}) = E - TS - \sum_{\text{species } i} \mu_i N_i = -T \ln Z_S$ .

In the applications of elementary  $e^+e^-$ ,  $pp$  and  $p\bar{p}$  collisions [31, 32], since the agreement between the experimental data and the results of statistical-thermal approach is poor in the strange sector, an additional parameter,  $\gamma_s$ , is required to suppress the thermal phase space of particles carrying strange or anti-strange quarks. Although the strangeness production is expected to be abundant in heavy-ion collisions, a number of analysis [33–38] have stated that a parameter called strangeness suppression factor,  $\gamma_s$ , is needed for a satisfactory description of the data. To be more precise, the applications of statistical-thermal method reproducing particle multiplicity in heavy-ion collisions and elementary particle collisions have unravelled that the canonical treatment is insufficient to quantify the strange particle yields observed in the experiments. Thus,  $\gamma_s$  is introduced to be responsible for the suppression of hadrons composed of strange and/or anti-strange quarks. This additional factor reduces the strange-particle phase space so that the agreement of the statistical-thermal method

results with the experimental data might be achieved [39, 40]. It is not wrong to say that  $\gamma_s = 1$  refers to complete strangeness saturation meaning that the system is free from strangeness suppression.

In the analysis, it is found that the strangeness saturation increases with the size of the system at all energies and  $\gamma_s$  increases with the participant number in the heavy-ion collisions [41]. However, the nucleon-nucleon center-of-mass energy dependency of  $\gamma_s$  given in Figure 3.1 [42] shows that  $\gamma_s$  is fairly constant but does not have a certain pattern.

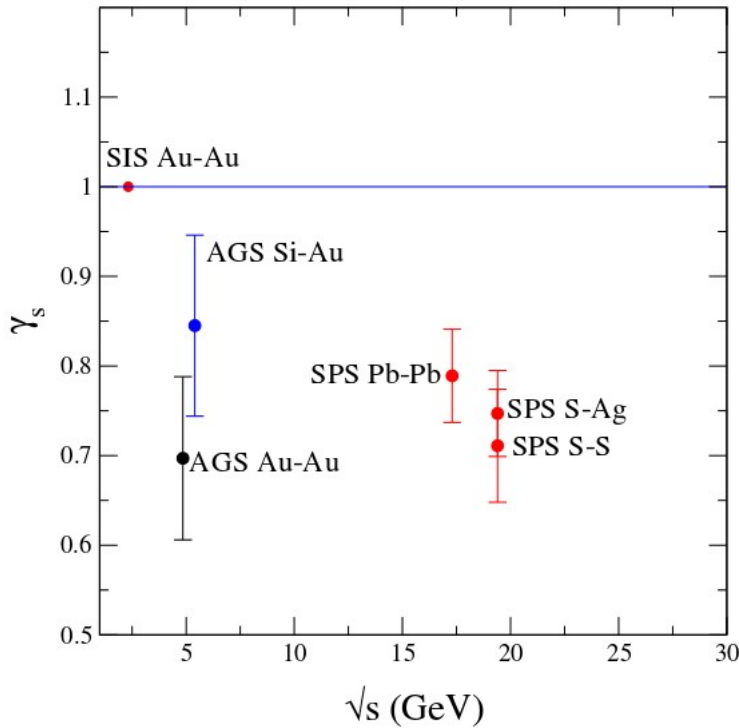


**Figure 3.1:** The nucleon-nucleon center-of-mass energy dependency of strangeness suppression factor,  $\gamma_s$  [42].

However, in the statistical-thermal approach, this  $\gamma_s$  factor does not suffice for the medium to reach to thermal equilibrium. As a solution, in [39] two volume parameters are suggested. The first one is the volume ( $V$ ) of the fireball at freeze out stage that is competitive with the volume of the grand canonical particle densities. The other one is the correlation volume ( $V_C$ ) that ensures the exact conservation of strangeness as it is in the canonical ensemble. In the analysis of statistical-thermal approach, the volume  $V$  is chosen smaller than the  $V_C$  in general.

## 3.2 THERMUS

The statistical-thermal model has been extremely successful [43–45] in the production of hadron multiplicities in both relativistic heavy-ion and elementary particle collisions. The achievement of this approach has pioneered to the design of various software codes [46,47].

A thermal model package for ROOT, (THERMUS) [12], one of these software codes, is a package designed with C++ classes and functions allowing analysis of the statistical-thermal approach to be performed within ROOT framework. Recent applications of THERMUS can be found in [44,48–55].

All mesons and baryons listed in the July 2002 Particle Physics Booklet are provided by THERMUS [56]. A decay list is also included for unstable particles featured in this list. Calculations of primordial thermal densities in THERMUS are made by performing numerical integrations or by evaluating Bessel functions if Boltzmann approximation is used in the grand canonical ensemble.

The statistical-thermal method can handle both the calculation of primary and secondary particles in heavy-ion collisions. Primary particles, by definition, are the ones directly produced from a thermal system whereas secondary particles, called decays, originate from the short-living resonances and feed stable hadrons. Depending on the approach, a number of thermal parameters and thermalized particles are used as input and a set of thermal quantities with the contribution of resonance decays is the output for given particles.

The fit between the prediction and experimental data is an essential operation for the analysis based on the statistical-thermal approach. In this case, experimental measurements are input and the statistical parameters which suit best with the experimental data is output.

THERMUS is able to make calculations within three statistical ensembles; grand-canonical ensemble which allows to fluctuate the conserved quantum numbers -Baryon (B), Strangeness (S) and Charge (Q)- on average; a canonical ensemble imposing all the quantum numbers to be conserved exactly and finally a mixed or strangeness canonical ensemble which is a combination of the canonical treatment of

strangeness and grand canonical treatment of quantum numbers B and Q.

(a) The grand-canonical ensemble used in THERMUS has following eight parameters:

$$T, \mu_B, \mu_S, \mu_Q, \mu_C, \gamma_S, \gamma_C, R.$$

Here T represents the temperature of the system,  $\mu_B$ ,  $\mu_S$  and  $\mu_Q$  are the baryon, strangeness and charge chemical potentials, respectively.  $\gamma_S$  is strangeness saturation factor,  $\gamma_C$  is charm saturation factor and finally R is the radius of the fireball.  $\gamma_C$  which has similar role with  $\gamma_S$  is fixed to 1 by THERMUS since the mechanism including particles with charm quark is out of the scope of the relevant collision system.

(b) The strangeness-canonical ensemble has following six parameters in THERMUS:

$$T, \mu_B, \mu_Q, \gamma_S, R_C, R.$$

$R_C$  is the correlation or the canonical radius in which the strangeness is exactly conserved. It is a natural result of the correlation volume ( $V_C$ ) given in the previous section.

(c) The canonical ensemble with exact conservation of B, S and Q, contains following six parameters:

$$T, B, S, Q, \gamma_S, R.$$

B, S and Q are baryon, strangeness and charge quantum numbers, respectively. Since all conservation is expected to be exact, there is no need for chemical potentials allowing fluctuations [25].

### 3.3 SHARE

SHARE (Statistical HAdronization with REsonances) [46] is a set of programs capable of accomplishing statistical analysis of particle yields created in the relativistic heavy-ion collisions. With the specification of statistical parameters as input, SHARE can generate the hadron abundances. All cascade decays of resonances can be obtained in the code that the Particle Data Tables (PDG) confirms. SHARE can provide a number of thermodynamic variables of the fireball. Depending on the statistical approach, the distributions of stable particles and hadronic resonances at the freeze-out point are calculated by evaluating a set of Bessel functions. An interface using

MINUIT [57] is provided for fitting the parameters to the experimental data. The programming language of SHARE is FORTRAN 77 whereas THERMUS uses C++ classes and functions.



## 4. ANALYSIS

As given in section 2.5, there are only a few studies using statistical-thermal approach to reproduce the ALICE data. In the attempt to compensate this deficiency in experimental high energy physics, a set of analysis implemented with both STAR and ALICE data has been conducted.

In the analysis, three distinct collision systems have been used to individually represent small, medium and large sized systems; pp, dAu, AuAu systems for STAR and PbPb systems for ALICE, respectively.

The canonical ensemble which is favorable for systems in smaller size is used for pp system. The strangeness canonical ensemble is implemented for not only pp system at higher energies but also for dAu and PbPb systems. Finally the grand canonical ensemble is preferred for AuAu and PbPb collisions and also in some cases for dAu system [25].

The particle yield measured in the experiments is defined as the number of particles per unit volume per unit rapidity per event. The particle ratios used in the THERMUS calculations are composed of these particle yields.

There are some reasons why specific particle ratios with different quark contents and different species are selected for the analysis. First, since the enhancement of the number of strange quarks is a signal of the QGP existence, the studies conducted with the ratios of strange to non-strange mesons are thought to be important for this phenomenon. In this context, the change in the value of  $K/\pi$  ratio is associated with the onset of deconfinement [58]. Also, a possible increase in the number of baryon/meson ratios gives the knowledge about if the measurement is related to a baryon dominated region or vice-versa [59].

$T_{ch}$  and  $\mu_B$  are the chemical freeze-out parameters which will be defined basically in this thesis. Thus, a number of particle ratios are particularly selected for the extraction

of these two parameters in the analysis of statistical-thermal approach.

Antiparticle to particle ratios are sensitive probes for the extraction of baryon chemical potential. Namely, recalling that baryon chemical potential itself is a measure of net baryon density; as  $\mu_B$  vanishes ( $\mu_B = 0$ ) the density of the particles become identical to those of antiparticles. This corresponds to the situation which the ratio of antiparticle to particle equals to 1. However, it is expected that there is a negligible difference in the number of the yield of particles and the associated antiparticles in the collisions at LHC. The low net-baryon density in the collisions at LHC at chemical decoupling is thought to be the reason of this difference. Also, antiparticle/particle ratios are not sensitive to any change in contributions from the resonances because of the equivalence of the decay chains for particles and antiparticles [30].

For the determination of the chemical freeze-out temperature in heavy-ion collisions, the ratios with hadrons having different masses are suitable probes. As the mass difference between the particles in the numerator and denominator increases, the ratio gets more sensitive to the temperature changes in the medium [30].

Both primary and secondary particles yield have been included to all calculations executed by THERMUS [12].

The method carried on the analysis is as follows: a set of experimental data consisting of measured particle ratios is introduced to THERMUS. As a statistical-thermal model package, THERMUS generates the best fit parameters which are suitable for the given data set. Based on the best fit parameters, the new particle ratios are also calculated by THERMUS. The best fit parameters extracted by THERMUS in this analysis are  $T_{ch}$ ,  $\mu_B$ ,  $\mu_S$  and  $\mu_Q$ . Those free parameters are sometimes going to be called as fit-type parameters through this chapter.

Furthermore,  $\gamma_s$ ,  $R_C$  and  $R$  are kept as fixed-type (fixed) parameters meaning that they are initially defined by the user in the analysis.

Although  $\gamma_s$  does not have an exact value for a particular system as shown in Figure 3.1 in section 3, for having physical meaning, the value of  $\gamma_s$  is kept nearly constant for a given collision system.

Several attempts have been conducted for finding the best fixed parameters and

eventually, for every collision system, only the best values of  $R_C$  and  $R$  are presented. In these attempts, it is found that the strangeness and the grand canonical ensemble is independent of the size of the system whereas canonical ensemble is strictly dependent on  $R$ . Thus, for the systems the strangeness and the grand canonical ensembles are applied and  $R$  is fixed to a constant value for every system. However, the best value of  $R$  parameter in the canonical ensemble has been defined by the user by varying it and presented in this chapter.

Also, in order to utilize the results some analysis methods are developed. Namely, for most of the experimental data, the analysis related to a specific data group that do not give consistent results is repeated with subgroups. The decision for the splitting process of the given data group is done whether the subset has resonances or not. Also, the analysis is repeated with different ensembles to obtain better canonic description of the experimental results.

In the canonical ensemble which is only used for pp collision analysis, the quantum numbers baryon ( $B$ ) and charge ( $Q$ ) are fixed to 2 referring to quantum number conservation. Precisely, when two protons collide, since proton is a baryon, the system has a value of 2 baryon quantum numbers and this should be conserved after the collisions. Similarly, proton has +1 charge and this adds up to 2 when there are two protons in the system before the collision. Keeping in mind, the conservation laws impose charge quantum number to fix to 2 after the collision. Beside, strangeness ( $S$ ) is fixed to 0 since proton is a composite particle which does not have any strange quarks.

Finally, the relations between temperature and the other thermodynamic parameters used in the analysis are presented using an experimental ratio from STAR and ALICE experiment. The temperature dependency of the thermodynamic parameters are given under the condition of a fixed particle ratio.

The solid lines show the THERMUS predictions while closed circles refer to the experimental data in the plots presented in this chapter. At the bottom of the plots, the differences between the experimental data and the THERMUS results are also included.

## 4.1 Statistical-Thermal Model Analysis of STAR Experiment

Reproduction of the measurements from the STAR Experiment with THERMUS is thought to be a reference study before the analysis to be conducted for the ALICE data. Since the STAR Collaboration is engaging with the nature and the physical properties of QGP as well, the results are expected to be comparable with those of ALICE. The following three sections cover the THERMUS analysis repeated for pp, dAu and AuAu collisions at  $\sqrt{s} = 200$  GeV.

### 4.1.1 Proton-proton collisions

There are some recent studies predicting [60] and measuring [61] the strangeness production which is a valuable signature of QGP formation in pp collisions. Hence, the analysis of these systems provide basis for the studies of heavy-ion collisions.

In Figure 4.1, the THERMUS results where the canonical ensemble is used are compared to the STAR data in pp collisions at  $\sqrt{s} = 200$  GeV [62, 63]. The only fit parameter is, the chemical freeze-out temperature,  $T_{ch} = 158 \pm 0.5$  MeV. On the other hand,  $\gamma_S = 0.59$  and  $R = 4$  fm are the fixed parameters.

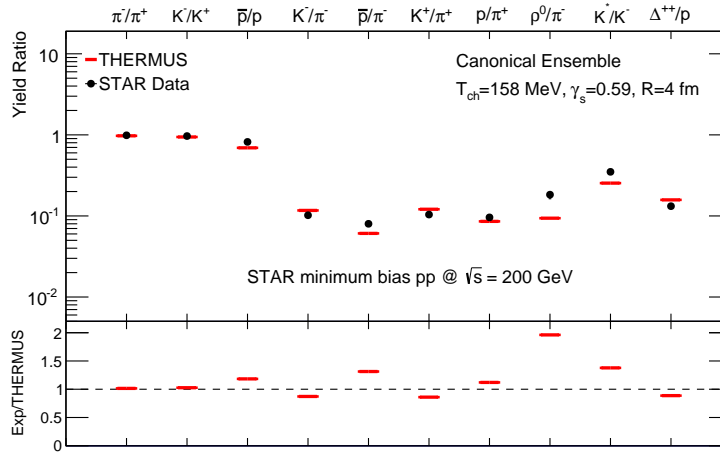


**Figure 4.1:** Comparison of the STAR data in pp collisions at  $\sqrt{s} = 200$  GeV [62, 63] and the THERMUS results. The canonical ensemble fit parameter is  $T_{ch} = 158 \pm 0.5$  MeV. The fixed parameters are  $\gamma_S = 0.59$  and  $R = 4$  fm.

The set of 10 particle ratios, given in Figure 4.1, is split into two for a better prediction. The analysis by using the canonical ensemble of the first seven ratios is in Figure 4.2. The fit parameter is  $T_{ch} = 167 \pm 2.4$  MeV and the fixed ones are  $\gamma_S = 0.5$  and  $R = 4.1$  fm.

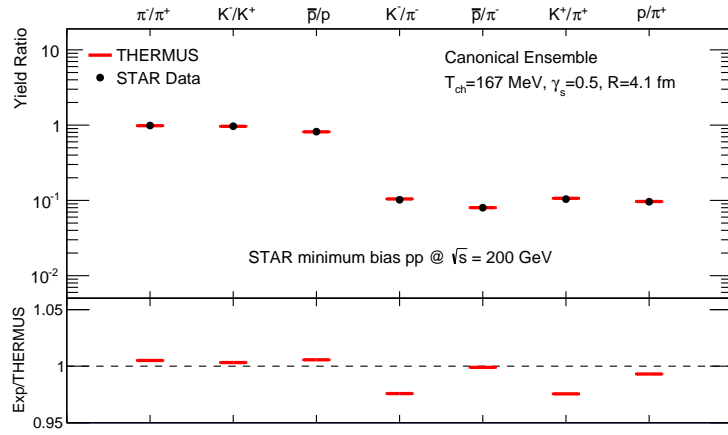


**Figure 4.2:** Comparison of the STAR data in pp collisions at  $\sqrt{s} = 200$  GeV [62] and the THERMUS results. The canonical ensemble fit parameter is  $T_{ch} = 167 \pm 2.4$  MeV. The fixed parameters are  $\gamma_S = 0.5$  and  $R = 4.1$  fm.

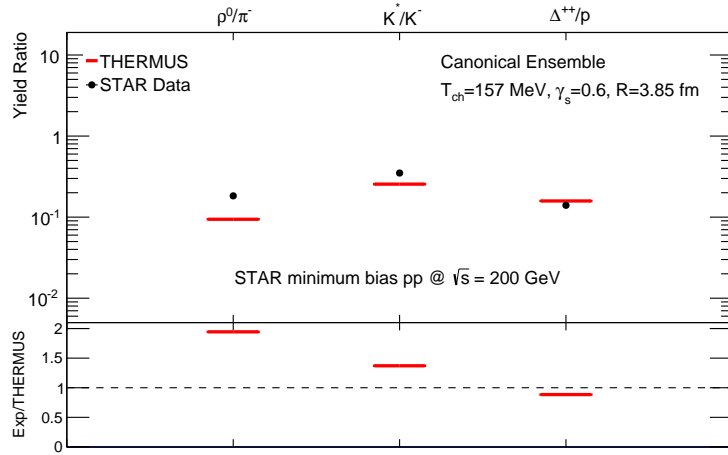


**Figure 4.3:** Comparison of the STAR data in pp collisions at  $\sqrt{s} = 200$  GeV [63] and the THERMUS results. The canonical ensemble fit parameter is  $T_{ch} = 157 \pm 0.6$  MeV. The fixed parameters are  $\gamma_S = 0.6$  and  $R = 3.85$  fm.

The second part of the given set is presented in Figure 4.3 which gives a better description of those in Figure 4.1. The fit parameter generated by the canonical ensemble is  $T_{ch} = 157 \pm 0.6$  MeV and  $\gamma_S = 0.6$  and  $R = 3.85$  fm are set to be the fixed-type.

#### 4.1.2 Deuterium-Gold collisions

As a transition medium from pp to heavy-ion collisions, Deuterium-Gold (dAu) systems are the assistive tools to give a proper description to the one of relativistic heavy-ion collisions. It is a must to meticulously evaluate the knowledge gathered

from this system. The STAR dAu measurements [62, 63] at  $\sqrt{s_{NN}} = 200$  GeV and its corresponding prediction values are shown in Figure 4.4 and Figure 4.5. The data set is almost the same - $\Sigma^*/\Lambda$  is added- with the one given for pp collisions. The calculations are repeated with two different ensembles.

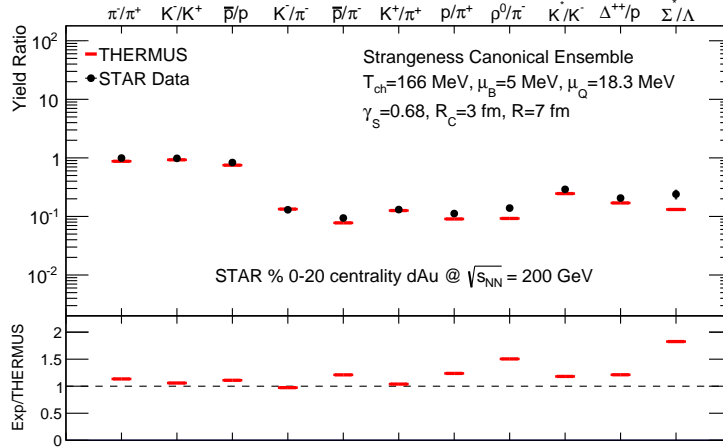


**Figure 4.4:** Comparison of the STAR data in dAu collisions at  $\sqrt{s_{NN}} = 200$  GeV [62, 63] and the THERMUS results. The strangeness canonical ensemble fit parameters are  $T_{ch} = 166 \pm 3.8$  MeV,  $\mu_B = 5 \pm 1.9$  MeV and  $\mu_Q = 18.3 \pm 3.3$  MeV and the fixed parameters are  $\gamma_S = 0.68$ ,  $R_C = 3$  fm and  $R = 7$  fm.

In Figure 4.4, the THERMUS results are accomplished by the strangeness canonical ensemble for the same data set. The fit parameters are  $T_{ch} = 166 \pm 3.8$  MeV,  $\mu_B = 5 \pm 1.9$  MeV and  $\mu_Q = 18.3 \pm 3.3$  MeV. The fixed parameters are  $\gamma_S = 0.68$ ,  $R_C = 3$  fm and  $R = 7$  fm.

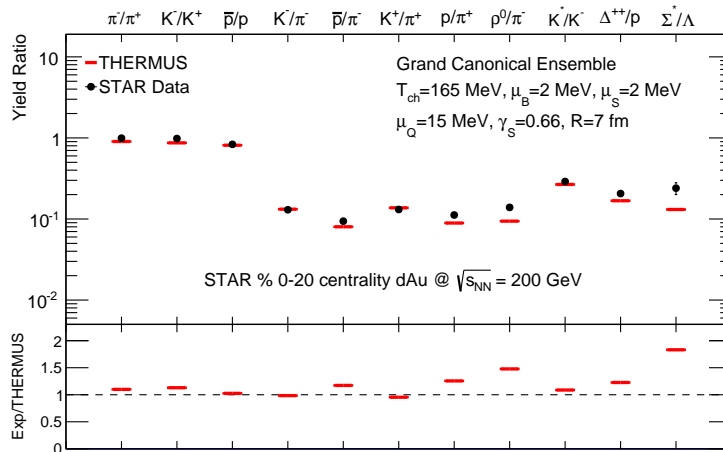


**Figure 4.5:** Comparison of the STAR data in dAu collisions at  $\sqrt{s_{NN}} = 200$  GeV [62, 63] and the THERMUS results. The grand canonical ensemble fit parameters are  $T_{ch} = 165 \pm 4$  MeV,  $\mu_B = 2 \pm 1$  MeV,  $\mu_S = 2 \pm 1$  MeV and  $\mu_Q = 15 \pm 3$  MeV while the fixed parameters are  $\gamma_S = 0.66$  and  $R = 7$  fm.

In Figure 4.5, the grand canonical ensemble is used with the following values. The fit parameters are  $T_{ch} = 165 \pm 4$  MeV,  $\mu_B = 2 \pm 1$  MeV,  $\mu_S = 2 \pm 1$  MeV and  $\mu_Q = 15 \pm 3$  MeV. The fixed parameters are  $\gamma_S = 0.66$  and  $R = 7$  fm.

As the set of 10 ratios was split into two distinct parts for pp analysis, similar method is repeated for previously given STAR dAu measurements at  $\sqrt{s_{NN}} = 200$  GeV to get a better fit. The first part of the data set is reproduced by two ensembles in Figure 4.6 and Figure 4.7.

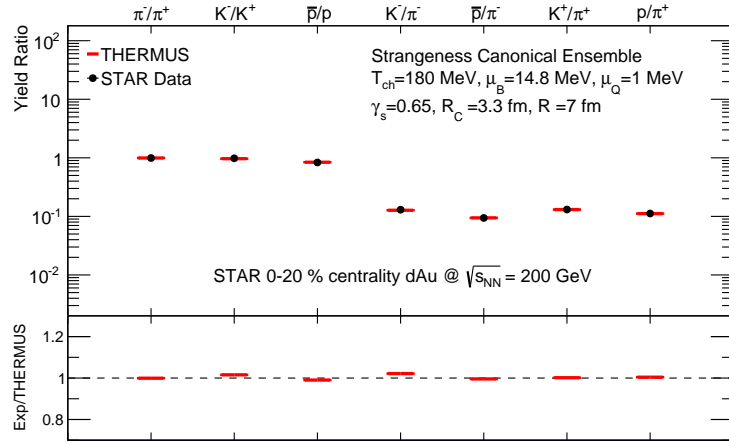


**Figure 4.6:** Comparison of the STAR data in dAu collisions at  $\sqrt{s_{NN}} = 200$  GeV [62] and the THERMUS results. The strangeness canonical ensemble fit parameters are  $T_{ch} = 180 \pm 5.6$  MeV,  $\mu_B = 14.8 \pm 6$  MeV and  $\mu_Q = 1 \pm 0.35$  MeV. The fixed-type parameters are  $\gamma_S = 0.65$ ,  $R_C = 3.3$  fm and  $R = 7$  fm.

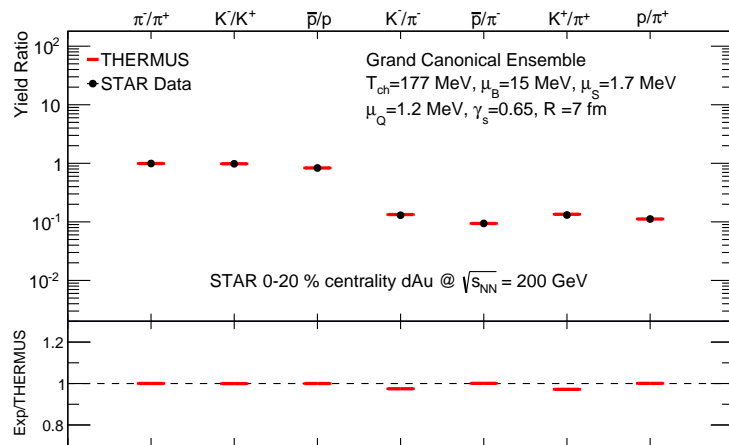


**Figure 4.7:** Comparison of the STAR data in dAu collisions at  $\sqrt{s_{NN}} = 200$  GeV [62] and the THERMUS results. The grand canonical ensemble fit parameters are  $T_{ch} = 177 \pm 6$  MeV,  $\mu_B = 15 \pm 6$  MeV,  $\mu_S = 1.7 \pm 0.5$  MeV,  $\mu_Q = 1.2 \pm 0.5$  MeV. The fixed-type parameters are  $\gamma_S = 0.65$  and  $R = 7$  fm.

In Figure 4.6, the strangeness canonical ensemble fit-type parameters are  $T_{ch} = 180 \pm 5.6$  MeV,  $\mu_B = 14.8 \pm 6$  MeV and  $\mu_Q = 1 \pm 0.35$  MeV where the fixed-type parameters are  $\gamma_s = 0.65$ ,  $R_C = 3.3$  fm and  $R = 7$  fm.

The grand canonical ensemble fit parameters for the given STAR data set in Figure 4.7 are  $T_{ch} = 177 \pm 6$  MeV,  $\mu_B = 15 \pm 6$  MeV,  $\mu_S = 1.7 \pm 0.5$  MeV,  $\mu_Q = 1.2 \pm 0.5$  MeV while the fixed parameters are  $\gamma_s = 0.65$  and  $R = 7$  fm.

In Figure 4.8, Other part of the data set taken from the STAR dAu measurements at  $\sqrt{s_{NN}} = 200$  GeV [63] is reproduced by THERMUS using the strangeness canonical ensemble. The fit parameters are  $T_{ch} = 163 \pm 10$  MeV,  $\mu_B = 40 \pm 6$  MeV,  $\mu_Q = 53.2 \pm 9$  MeV and the fixed parameters are  $\gamma_s = 0.7$ ,  $R_C = 2.3$  fm,  $R = 7$  fm.

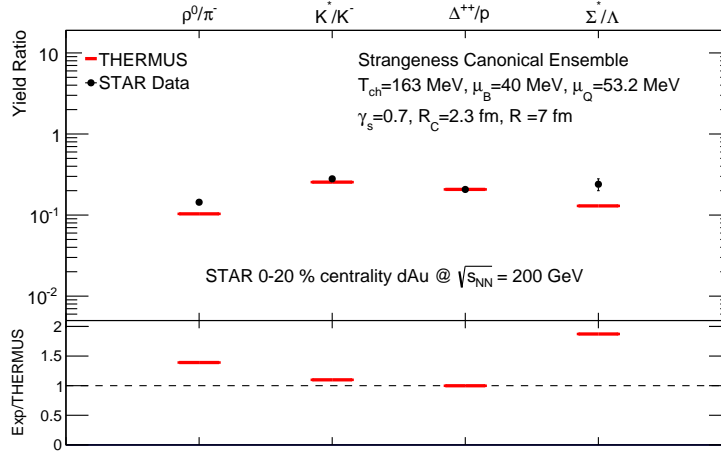


**Figure 4.8:** Comparison of the STAR data in dAu collisions at  $\sqrt{s_{NN}} = 200$  GeV [63] and the THERMUS results. The strangeness canonical ensemble fit parameters are  $T_{ch} = 163 \pm 10$  MeV,  $\mu_B = 40 \pm 6$  MeV,  $\mu_Q = 53.2 \pm 9$  MeV. The fixed parameters are  $\gamma_s = 0.7$ ,  $R_C = 2.3$  fm,  $R = 7$  fm.

### 4.1.3 Gold-Gold collisions

Collisions of relativistic heavy-ion, AuAu systems in particular, are used as approved probes for the investigation of QGP phase in both theoretical and experimental particle physics [64]. The THERMUS analysis reproducing the experimental data and its interpretation are expected to enhance the understanding of QGP formation and chemical freeze-out parameters.

First, a set of the STAR AuAu measurements at  $\sqrt{s_{NN}} = 200$  GeV [13] is used to compare with the THERMUS prediction. The data have the following  $p_T$  ranges:  $p_T$

of the quark is between 0.8-1.2 GeV that corresponds to the  $p_T$  range between 2.4-3.6 MeV for baryon and 1.6-2.4 MeV for meson [13].

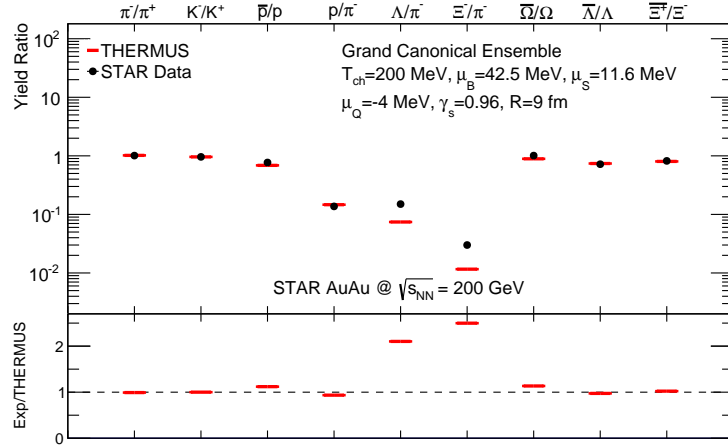


**Figure 4.9:** Comparison of the STAR data in AuAu collisions at  $\sqrt{s_{NN}} = 200$  GeV [13] and the THERMUS results. The grand canonical ensemble fit parameters are  $T_{ch} = 200 \pm 1.4$  MeV,  $\mu_B = 42.5 \pm 1.2$  MeV,  $\mu_S = 11.6 \pm 2.7$  MeV and  $\mu_Q = -4 \pm 0.7$  MeV. The fixed parameters are  $\gamma_S = 0.96$  and  $R = 9$  fm.

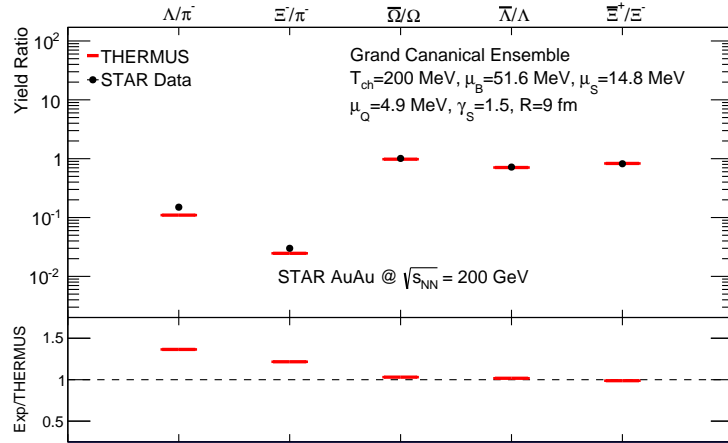


**Figure 4.10:** Comparison of the STAR data in AuAu collisions at  $\sqrt{s_{NN}} = 200$  GeV [13] and the THERMUS results. The grand canonical ensemble fit parameters are  $T_{ch} = 200 \pm 1.7$  MeV,  $\mu_B = 51.6 \pm 7$  MeV,  $\mu_S = 14.8 \pm 4.3$  MeV,  $\mu_Q = 4.9 \pm 2.3$  MeV. The fixed parameters are  $\gamma_S = 1.5$  and  $R = 9$  fm.

Since the given system is large enough for the quantum number fluctuations around the average values, results have a high confidence level in the grand canonical ensemble. Thus, the comparison of the STAR data [13] and the THERMUS results are presented in Figure 4.9 with the grand canonical ensemble fit parameters:  $T_{ch} = 200 \pm 1.4$  MeV,

$\mu_B = 42.5 \pm 1.2$  MeV,  $\mu_S = 11.6 \pm 2.7$  MeV and  $\mu_Q = -4 \pm 0.7$  MeV while  $\gamma_S = 0.96$  and  $R = 9$  fm are of fixed-type.

The ratios of resonance particles and  $\pi^-$  from the STAR data in Figure 4.9 are extracted to get a better fit. The corresponding grand canonical ensemble predictions are presented in Figure 4.10. The fit-type parameters are  $T_{ch} = 200 \pm 1.7$  MeV,  $\mu_B = 51.6 \pm 7$  MeV,  $\mu_S = 14.8 \pm 4.3$  MeV,  $\mu_Q = 4.9 \pm 2.3$  MeV and the fixed parameters are  $\gamma_S = 1.5$  and  $R = 9$  fm.

The particle ratios consisting of non-resonance baryons from the STAR measurements in AuAu collisions at  $\sqrt{s_{NN}} = 200$  GeV [62] are presented in Figure 4.11. The grand canonical ensemble fit parameters are  $T_{ch} = 173 \pm 5.8$  MeV,  $\mu_B = 22 \pm 4.6$  MeV,  $\mu_S = 2 \pm 0.6$  MeV and  $\mu_Q = 1 \pm 1.4$  MeV while the fixed values are  $\gamma_S = 0.8$ ,  $R = 9$  fm.

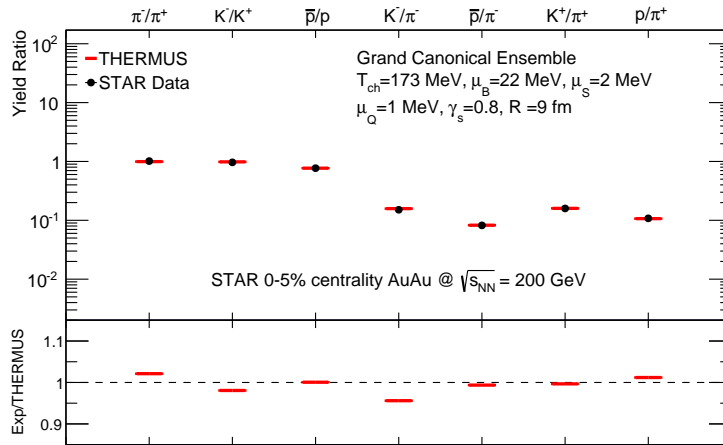


**Figure 4.11:** Comparison of the STAR data in AuAu collisions at  $\sqrt{s_{NN}} = 200$  GeV [62] and the THERMUS results. The grand canonical ensemble fit parameters are  $T_{ch} = 173 \pm 5.8$  MeV,  $\mu_B = 22 \pm 4.6$  MeV,  $\mu_S = 2 \pm 0.6$  MeV and  $\mu_Q = 1 \pm 1.4$  MeV. The fixed parameters  $\gamma_S = 0.8$ ,  $R = 9$  fm.

Finally, the relations between chemical freeze-out temperature and the other statistical-thermal parameters used in the analysis are sketched.  $T-\mu_B$ ,  $T-\mu_S$ ,  $T-\mu_Q$ ,  $T-\gamma_S$  and  $T-R$  dependency plots are shown in Figure 4.12, Figure 4.13, Figure 4.14, Figure 4.15 and Figure 4.16, respectively.

$\bar{p}/p = 0.769 \pm 0.055$  ratio taken from the STAR AuAu measurement [13] is forced to remain constant and the values of  $T$  and  $\mu_B$  parameters giving this explicit number are drawn in Figure 4.12. The grand canonical ensemble fixed parameters are  $\mu_S = 10$

MeV,  $\mu_Q = -5.2$  MeV,  $\gamma_S = 0.86$  and  $R = 9$  fm. These values are particularly selected because these are the results which give the experimental  $\bar{p}/p = 0.769 \pm 0.055$  ratio exactly.

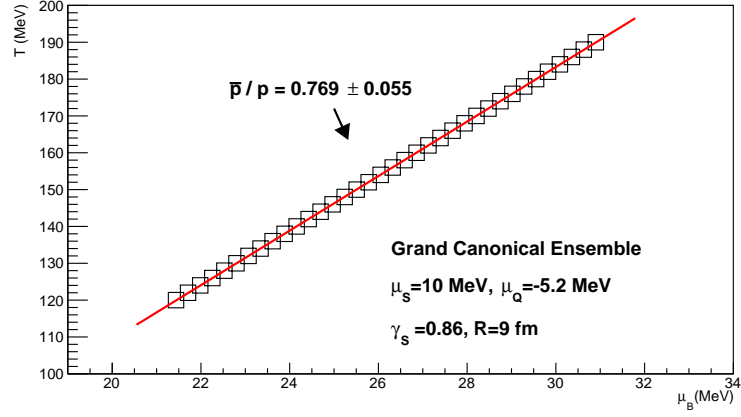


**Figure 4.12:**  $T$ - $\mu_B$  dependency plot under the condition of  $\bar{p}/p = 0.769 \pm 0.055$  ratio taken from the STAR data [13]. The grand canonical ensemble fixed parameters are  $\mu_S = 10$  MeV,  $\mu_Q = -5.2$  MeV,  $\gamma_S = 0.86$  and  $R = 9$  fm. The solid line represents the fit function  $T = 7.4\mu_B - 38.74$ .

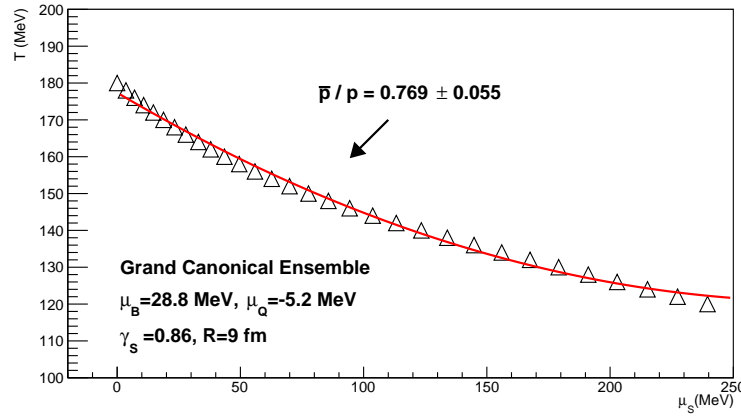


**Figure 4.13:**  $T$ - $\mu_S$  dependency plot under the condition of  $\bar{p}/p = 0.769 \pm 0.055$  ratio taken from the STAR data [13]. The grand canonical ensemble fixed parameters:  $\mu_B = 28.8$  MeV,  $\mu_Q = -5.2$  MeV,  $\gamma_S = 0.86$  and  $R = 9$  fm. The solid line represents the fit function  $T = 0.00068\mu_S^2 - 0.394\mu_S + 177.38$ .

Similar method is followed for  $T$ - $\mu_S$ ,  $T$ - $\mu_Q$ ,  $T$ - $\gamma_S$  and  $T$ - $R$  relations. Figure 4.13 gives the relation between  $T$  and  $\mu_Q$  while  $\bar{p}/p$  ratio is kept at  $0.769 \pm 0.055$  using the grand canonical ensemble fixed parameters;  $\mu_B = 28.8$  MeV,  $\mu_Q = -5.2$  MeV,  $\gamma_S = 0.86$  and  $R = 9$  fm. Then, Figure 4.14 represents  $T$ - $\mu_Q$  dependency when  $\bar{p}/p$  ratio is fixed to

$0.769 \pm 0.055$ . The grand canonical ensemble fixed parameters:  $\mu_B = 28.8$  MeV,  $\mu_S = 10$  MeV,  $\gamma_s = 0.86$  and  $R = 9$  fm.

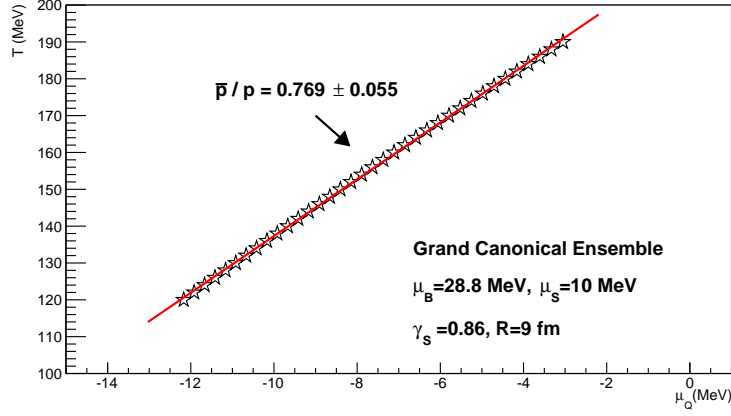


**Figure 4.14:**  $T-\mu_Q$  dependency plot under the condition of  $\bar{p}/p = 0.769 \pm 0.055$  ratio taken from the STAR data [13]. The grand canonical ensemble fixed parameters:  $\mu_B = 28.8$  MeV,  $\mu_S = 10$  MeV,  $\gamma_s = 0.86$  and  $R = 9$  fm. The solid line represents the fit function  $T = 7.7\mu_Q + 214.3$ .

Also, the relation between  $T$  and  $\gamma_s$  is sketched in Figure 4.15 where the  $\bar{p}/p$  ratio is kept at  $0.769 \pm 0.055$  using the grand canonical ensemble fixed parameters  $\mu_B = 28.8$  MeV,  $\mu_S = 10$  MeV,  $\mu_Q = -5.2$  MeV and  $R = 9$  fm.

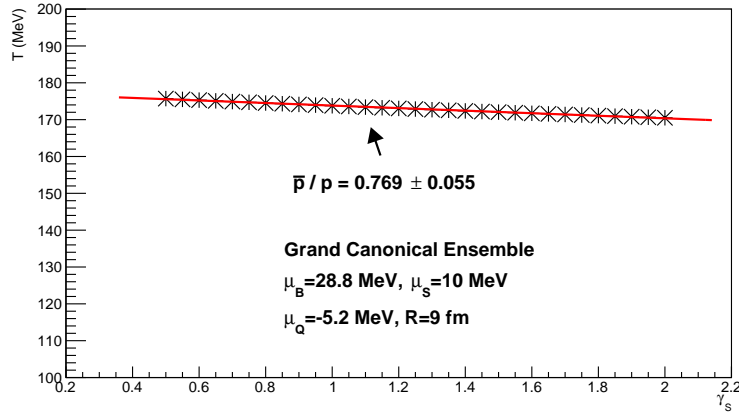


**Figure 4.15:**  $T-\gamma_s$  dependency plot under the condition of  $\bar{p}/p = 0.769 \pm 0.055$  ratio taken from the STAR data [13]. The grand canonical ensemble fixed parameters:  $\mu_B = 28.8$  MeV,  $\mu_S = 10$  MeV,  $\mu_Q = -5.2$  MeV and  $R = 9$  fm. The solid line represents the fit function  $T = -3.46\gamma_s + 177.2$ .

Finally, THERMUS results for  $T-R$  dependency are shown in Figure 4.16.  $\bar{p}/p$  ratio is fixed to  $0.769 \pm 0.055$  while the grand canonical fixed parameters are  $\mu_B = 28.8$  MeV,  $\mu_S = 10$  MeV,  $\mu_Q = -5.2$  MeV and  $\gamma_s = 0.86$ .

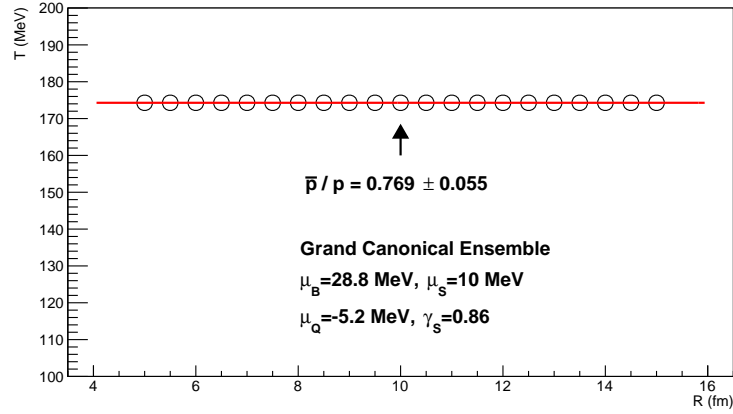


**Figure 4.16:** T-R dependency plot under the condition of  $\bar{p}/p = 0.769 \pm 0.055$  ratio taken from the STAR data [13]. The grand canonical ensemble fixed parameters:  $\mu_B = 28.8$  MeV,  $\mu_S = 10$  MeV,  $\mu_Q = -5.2$  MeV and  $\gamma_S = 0.86$ . The solid line represents the fit function  $T = 174.28$ .

## 4.2 Statistical-Thermal Model Analysis of ALICE Experiment

The analysis of the STAR measurements presented so far is supposed to be a reference study to help understanding the collisions, particularly the mechanism of QGP formation, created in LHC. In the light of this reference study together with the analysis predicting the ALICE data lying in a wider energy range from 0.9 TeV to 2.76 TeV, it is thought that these predictions will help to unravel the thermal properties of QGP.

### 4.2.1 Proton-proton collisions

Since the pp system has smaller size, the canonical ensemble is favorable in the application of THERMUS for pp collisions at lower center of mass energies. However, the strangeness canonical ensemble calculations give reasonable results for the pp collisions at relatively high energy regime.

The ALICE data in pp collisions at  $\sqrt{s} = 0.9$  TeV [65] which consists of 7 ratios of non-resonance particles and their corresponding THERMUS results are shown in Figure 4.17. The measurements are taken at the range of central rapidity  $|y| < 0.5$ . The canonical ensemble fit parameter in Figure 4.17 is  $T_{ch} \simeq 156$  MeV while the fixed-types are  $\gamma_S = 0.6$  and  $R = 7.2$  fm.

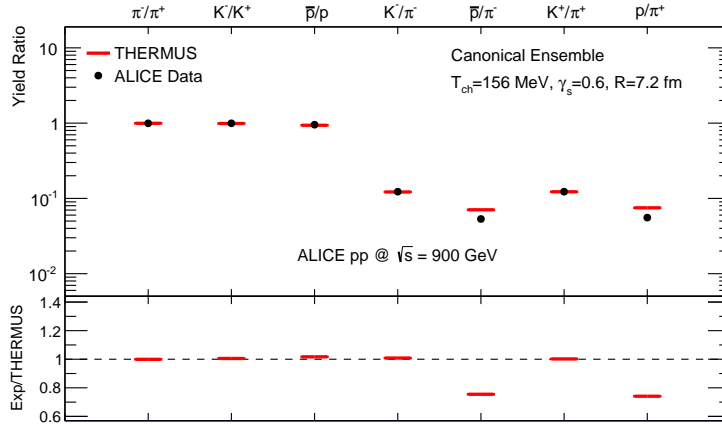


**Figure 4.17:** Comparison of the ALICE data in pp collisions at  $\sqrt{s} = 900 \text{ GeV}$  [65] and the THERMUS prediction. The canonical ensemble fit parameter is  $T_{ch} \simeq 156 \text{ MeV}$  and the fixed parameters are  $\gamma_s = 0.6$  and  $R = 7.2 \text{ fm}$ .

In Figure 4.18, the prediction is repeated for the strangeness canonical ensemble with the same data group given in the previous plot. The fit parameters are  $T_{ch} = 146 \pm 4 \text{ MeV}$ ,  $\mu_B = 2.9 \pm 1.2 \text{ MeV}$  and  $\mu_Q = 0.61 \pm 0.4 \text{ MeV}$ . The fixed-type parameters are  $\gamma_s = 0.67$ ,  $R_C = 4.3 \text{ fm}$  and  $R = 6.5 \text{ fm}$ .

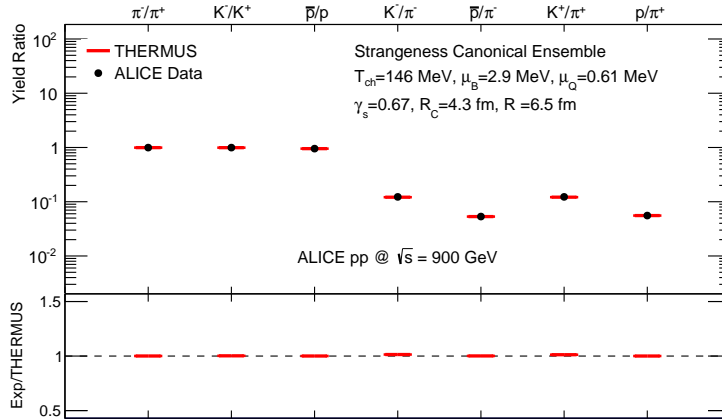


**Figure 4.18:** Comparison of the ALICE data in pp collisions at  $\sqrt{s} = 900 \text{ GeV}$  [65] and the THERMUS results. The strangeness canonical ensemble fit parameters are  $T_{ch} = 146 \pm 4 \text{ MeV}$ ,  $\mu_B = 2.9 \pm 1.2 \text{ MeV}$  and  $\mu_Q = 0.61 \pm 0.4 \text{ MeV}$ . The fixed parameters are  $\gamma_s = 0.67$ ,  $R_C = 4.3 \text{ fm}$  and  $R = 6.5 \text{ fm}$ .

## 4.2.2 Lead-Lead collisions

PbPb systems in the relativistic heavy-ion collisions enable to search for the QGP formation and investigate deeply its properties. The analysis which predicts

the experimental data is critically important to reveal the real success of the statistical-thermal approach. Therefore, the reproduction of the ALICE PbPb measurement at  $\sqrt{s_{NN}} = 2.76$  TeV is performed meticulously.

The data set is arranged from the ALICE data in PbPb collisions at  $\sqrt{s_{NN}} = 2.76$  TeV [66] with the range of central rapidity  $|y| < 0.5$ . Also, the ratios of  $\Lambda/K_S^0$  with 0-5 % centrality [67] and the ratios of  $\Xi^+/\Xi^-$ ,  $\Omega^+/\Omega^-$  [68] have been included to the data group.

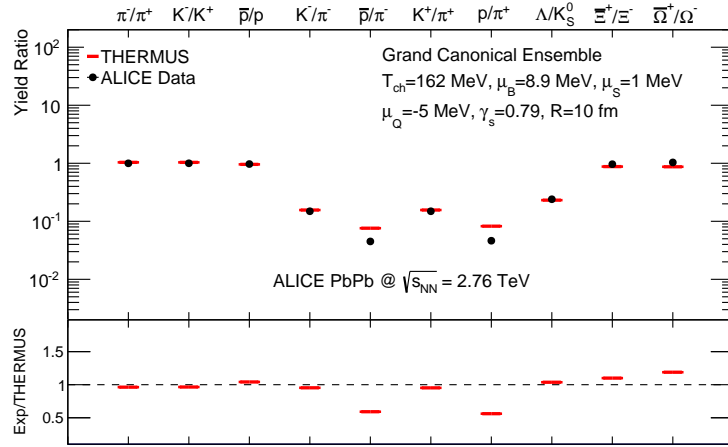


**Figure 4.19:** Comparison of the ALICE data in PbPb collisions at  $\sqrt{s_{NN}} = 2.76$  TeV [67–69] and the THERMUS results. The grand canonical ensemble fit parameters are  $T_{ch} = 162 \pm 0.9$  MeV,  $\mu_B = 8.9 \pm 0.24$  MeV,  $\mu_S = 1 \pm 0.1$  MeV and  $\mu_Q = -5 \pm 0.43$  MeV. The fixed parameters are  $\gamma_s = 0.79$  and  $R = 10$  fm.

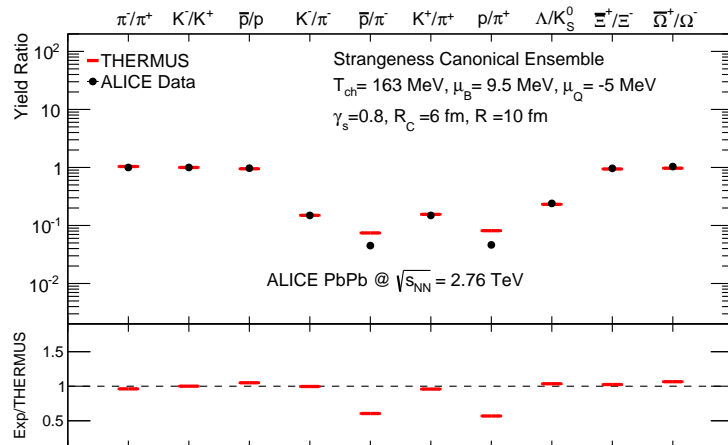


**Figure 4.20:** Comparison of the ALICE data in PbPb collisions at  $\sqrt{s_{NN}} = 2.76$  TeV [67–69] and the THERMUS results. The strangeness canonical ensemble fit parameters are  $T_{ch} = 163 \pm 0.5$  MeV,  $\mu_B = 9.5 \pm 0.9$  MeV and  $\mu_Q = -5 \pm 0.2$  MeV. The fixed parameters are  $\gamma_s = 0.8$ ,  $R_C = 6$  fm,  $R = 10$  fm.

Both resonance and non-resonance baryons are included to the group of particle ratios taken from the ALICE PbPb measurements at  $\sqrt{s_{NN}} = 2.76$  TeV. The THERMUS fits from the grand canonical and strangeness canonical ensembles are shown in Figure 4.19 and Figure 4.20, respectively.

In Figure 4.19, the fit parameters used for the grand canonical ensemble are  $T_{ch} = 162 \pm 0.9$  MeV,  $\mu_B = 8.9 \pm 0.24$  MeV,  $\mu_S = 1 \pm 0.1$  MeV and  $\mu_Q = -5 \pm 0.43$  MeV where the fixed values are  $\gamma_S = 0.79$ ,  $R = 10$  fm.

In Figure 4.20, the fit parameters used for the strangeness canonical ensemble are  $T_{ch} = 163 \pm 0.5$  MeV,  $\mu_B = 9.5 \pm 0.9$  MeV and  $\mu_Q = -5 \pm 0.2$  MeV where the fixed values are  $\gamma_S = 0.8$ ,  $R_C = 6$  fm,  $R = 10$  fm.

At the end of the analysis of STAR data, the relations between temperature and other statistical-thermal model parameters have been presented. Same method is followed for the  $\bar{p}/p$  ratio taken from the ALICE PbPb measurements at  $\sqrt{s_{NN}} = 2.76$  TeV [66]. The  $\bar{p}/p$  ratio,  $0.9705 \pm 0.012$ , is held constant and the change in the T and  $\mu_B$  is drawn in Figure 4.21. The parameters which gives this exact particle ratio are  $\mu_S = 1$  MeV,  $\mu_Q = -2.8$  MeV,  $\gamma_S = 0.81$  and  $R = 10$  fm.

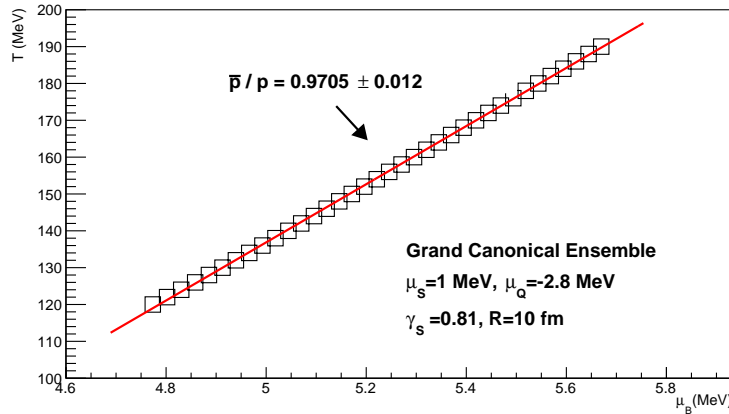


**Figure 4.21:**  $T$ - $\mu_B$  dependency plot under the condition of  $\bar{p}/p = 0.9705 \pm 0.012$  taken from the ALICE data in PbPb collisions at  $\sqrt{s_{NN}} = 2.76$  TeV [66]. The grand canonical ensemble fixed parameters of  $\mu_S = 1$  MeV,  $\mu_Q = -2.8$  MeV,  $\gamma_S = 0.81$  and  $R = 10$  fm. The solid line represents the fit function  $T = 78.9\mu_B - 257.73$ .

Similar method described for Figure 4.21 is followed for the following relations;  $T$ - $\mu_Q$ ,  $T$ - $\gamma_S$  and  $T$ - $R$  in Figure 4.22, Figure 4.23 and Figure 4.24 , respectively.

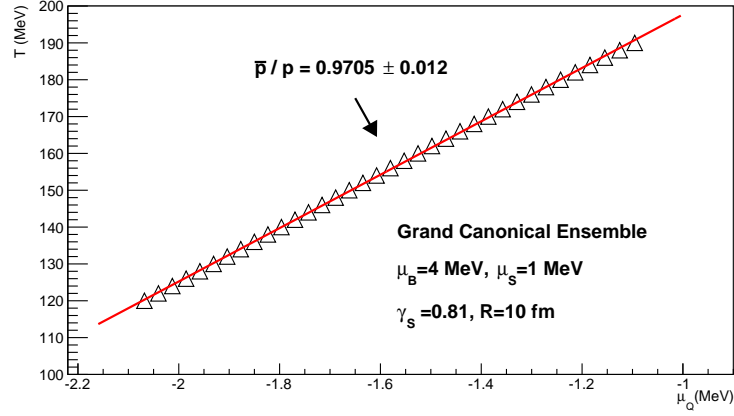


**Figure 4.22:**  $T-\mu_Q$  dependency plot under the condition of  $\bar{p}/p = 0.9705 \pm 0.012$  taken from the ALICE data in PbPb collisions at  $\sqrt{s_{NN}} = 2.76$  TeV [66]. The grand canonical ensemble fixed parameters are  $\mu_B = 4$  MeV,  $\mu_S = 1$  MeV,  $\gamma_S = 0.81$  and  $R = 10$  fm. The solid line represents the fit function  $T = 72.46\mu_Q + 270.15$ .

$T-\mu_Q$  plot shown in Figure 4.22 is obtained with the grand canonical ensemble fixed-type parameters  $\mu_B = 4$  MeV,  $\mu_S = 1$  MeV,  $\gamma_S = 0.81$  and  $R = 10$  fm.

In Figure 4.23,  $T-\gamma_S$  plot is shown with the grand canonical ensemble fixed parameters  $\mu_B = 4$  MeV,  $\mu_S = 1$  MeV,  $\mu_Q = -2.8$  MeV and  $R = 10$  fm.

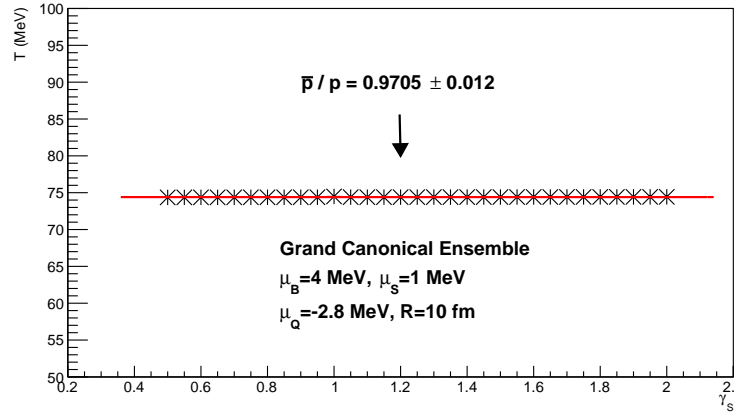


**Figure 4.23:**  $T-\gamma_S$  dependency plot under the condition of  $\bar{p}/p = 0.9705 \pm 0.012$  taken from the ALICE data in PbPb collisions at  $\sqrt{s_{NN}} = 2.76$  TeV [66]. The grand canonical ensemble fixed parameters are  $\mu_B = 4$  MeV,  $\mu_S = 1$  MeV,  $\mu_Q = -2.8$  MeV and  $R = 10$  fm. The solid line represents the fit function  $T = 74.4$ .

Finally, in Figure 4.24, the plot giving the relation between the parameters  $T$  and  $R$  is shown. The values are extracted from the grand canonical ensemble calculations. The

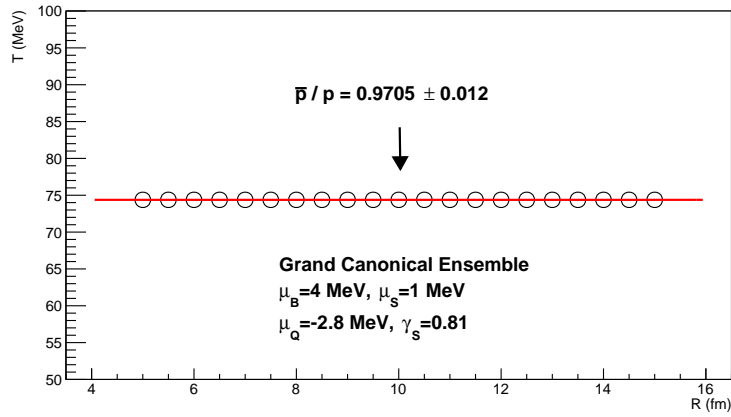


**Figure 4.24:** T-R dependency plot under the condition of  $\bar{p}/p = 0.9705 \pm 0.012$  taken from the ALICE data in PbPb collisions at  $\sqrt{s_{NN}} = 2.76$  TeV [66]. The grand canonical ensemble fixed parameters are  $\mu_B = 4$  MeV,  $\mu_S = 1$  MeV,  $\mu_Q = -2.8$  MeV,  $\gamma_S = 0.81$ . The solid line represents the fit function  $T = 74.38$ .

fixed parameters which THERMUS executed are  $\mu_B = 4$  MeV,  $\mu_S = 1$  MeV,  $\mu_Q = -2.8$  MeV and  $\gamma_S = 0.81$ .

Although  $\mu_S = 1$  MeV is taken in the calculations of the grand canonical ensemble, the result about the relation between T and  $\mu_S$  is not reasonable so T- $\mu_S$  plot is not included to the analysis. As a result,  $\mu_S$  does not play an effective role in this analysis and it can be even ignored.

The interpretation of the plots giving the comparison of experimental data and the THERMUS predictions and the interpretation of the dependency plots can be found in the following chapter.

## 5. RESULTS

All the STAR and the ALICE data together with their THERMUS predictions and the temperature dependencies of statistical-thermal parameters are presented in section 4. In this chapter, the evaluation of these results can be found in a detail.

In general, when the non-resonance and resonance hadrons are treated separately, as it can be seen from the analysis, the results obviously get better than the previous non-split versions.

In the former data analysis, there is no THERMUS prediction for the STAR data in dAu collisions. This study is the first one to give predictions for the STAR data in dAu collisions at  $\sqrt{s} = 200$  GeV. Looking at these results, the THERMUS predictions are solid enough to describe the experimental ratios which deserves a credit for the heavy-ion results. Also, for both analysis of pp and dAu collisions, the THERMUS results are successful in reproducing all the ratios except  $\Sigma^* / \Lambda$  and  $\rho^0 / \pi^-$ .

A possible solution for these deviations is a correction of primary and secondary yield for both  $\Lambda$  and  $\rho^0$  particles. In analysis of statistical-thermal method, as stated before, both primary and secondary particle contributions are included to the calculations since the experimental total particle yields measured by the detectors include feed-down yields. Feed-down yields include decay contributions coming from heavier hadrons and hadronic resonances. However, THERMUS has a capability that allows the primordial particles not to decay so the secondary particles are vanished by the approach. This application is called feed-down correction and it gives the opportunity not to take into account the contributions from resonance particles. It is thought that this correction can improve the results for  $\Sigma^* / \Lambda$  and  $\rho^0 / \pi^-$ .

In the analysis of STAR AuAu measurement featured in section 4.3, the THERMUS predictions are quite solid in describing the experimental data including the resonances. On the other hand, the previous THERMUS results done for the STAR data in AuAu collisions at  $\sqrt{s_{NN}} = 200$  GeV shown in Figure 2.3 fails to predict the ratios with

resonances.

Since pp collisions at STAR at  $\sqrt{s} = 200$  GeV is a small system at low energy regime, the THERMUS results given by strangeness canonical ensemble do not fit the data and the comparison plot is not included to the work. This poor description implies that the given system does not allow quantum numbers -B and Q- to fluctuate around the average values even if the quantum number S is behaved canonically. However, the results from strangeness canonical ensemble for STAR data are as accurate as the results of both canonical and grand canonical ensembles.

The THERMUS calculations for the STAR data performed in the analysis section is quite successful. Therefore, it is not wrong to say that these results might be baseline for the studies to be conducted particularly for ALICE Physics.

In the analysis of the ALICE measurements in pp collisions at  $\sqrt{s} = 900$  GeV, the strangeness canonical ensemble is slightly more successful than the canonical treatment. The lack of the strangeness treatment of the STAR data in pp collisions at  $\sqrt{s} = 200$  GeV has an important outcome that the higher the energy of the pp collisions is, the more tendency to tolerate the quantum number fluctuations in the system.

When it comes to ALICE PbPb collisions at  $\sqrt{s_{NN}} = 2.76$  TeV, as it can be seen from Figure 4.25 and Figure 4.26, both grand canonical and strangeness canonical approach are quite successful in describing experimental data except the ratios of  $\bar{p}/\pi^-$  and  $p/\pi^+$ . The feed-down correction might be a solution to improve these ratios as well.

The relation between temperature and other statistical-thermal parameters has been studied using STAR data.  $T-\mu_B$  plot given in Figure 4.12 reflects the fact that there is a linear relation between these two statistical parameters meaning that  $\mu_B$  is directly proportional to T. Figure 4.13 gives the relation between  $T-\mu_S$  which means that  $\mu_S$  decreases with the temperature. The data in the  $T-\mu_Q$  plot in Figure 4.14 has a linear behavior where  $\mu_Q$  increases with the temperature. However, the relation between T and  $\gamma_S$  in Figure 4.15 reflects that  $\gamma_S$  is almost independent of T with a small negative slope.

The temperature dependency of the parameters used in the analysis are also studied with the ratio taken from ALICE data. Both the  $T-\mu_B$  and  $T-\mu_S$  plots have almost the same trend. Namely,  $\mu_B$  and  $\mu_Q$  are decreasing with the temperature which can be seen

from Figure 4.27 and Figure 4.28. Also, the parameters  $\gamma_S$  and  $R$  are independent of the temperature as shown in Figure 4.29 and Figure 4.30.

The chemical potentials,  $\mu_B$  and  $\mu_Q$  increase as the temperature increases since the number of both baryons and charged particles increase with the temperature. Precisely, recalling the definitions of baryon chemical potential,  $\mu_B$  controls the difference in the number of baryons and anti-baryons in the system. Similarly,  $\mu_Q$  controls the difference in the number of charged and anti-charged particles in the system. The response of  $\mu_B$  and  $\mu_Q$  to the temperature increase have also a tendency to increase in order to balance the temperature change. This fact verifies the temperature dependency plots related to those chemical potentials given in the analysis section. However,  $\mu_S$  is inversely proportional to the temperature as shown in the analysis section. This situation implies a blurred issue in the strange sector.

When the temperature changes, the radius of the fireball  $R$  stays the same since the volume factor  $R$  cancels in the ratio calculations. However, this is valid only when the strangeness and grand canonical ensemble are used for the calculations. On the other hand, the canonical ensemble predictions are quite sensitive to the volume changes since the system is small sized.

To conclude, as an ultimate goal of this thesis study, a general picture can be drawn by using the results of the complete analysis. The relations between baryon chemical potential, chemical freeze-out temperature and the center of mass energy are individually sketched in the following two plots. The point which needs to be paid attention is  $\mu_B$  and  $T_{ch}$  values in Figure 5.1 and Figure 5.2 are extracted from the same analysis for every given system. Namely, they are not independent of each other which is vital requirement of physical consistency. The statistical-thermal parameters,  $T_{ch}$  and  $\mu_B$  are taken from the data in Figure 4.4, Figure 4.11, Figure 4.18 and Figure 4.22 given in the previous chapter.

The relation between baryon chemical potential and center of mass energy is shown in Figure 5.1.  $\mu_B = 5 \pm 1.9$  MeV and  $\mu_B = 22 \pm 4.6$  MeV are extracted from the analysis of STAR data in dAu collisions and in AuAu collisions at the center of mass energy of 200 GeV, respectively. Also,  $\mu_B = 2.9 \pm 1.3$  MeV is from the analysis of ALICE data

in pp collisions at  $\sqrt{s} = 900$  GeV and finally  $\mu_B = 9.5 \pm 0.9$  MeV is from the analysis of ALICE data in PbPb collisions at  $\sqrt{s_{NN}} = 2.76$  TeV.

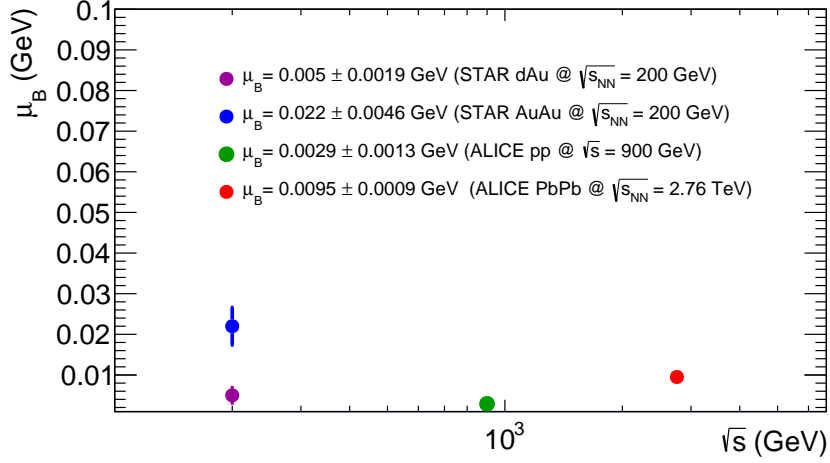


**Figure 5.1:** The center of mass energy dependency of baryon chemical potential. See text for details.

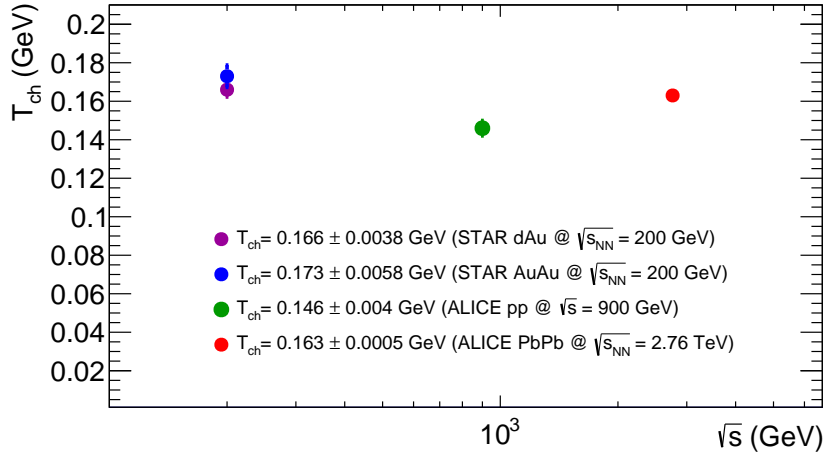


**Figure 5.2:** The center of mass energy dependency of chemical freeze-out temperature. See text for details.

Then, in a similar fashion, the relation between chemical freeze-out temperature ( $T_{ch}$ ) and center of mass energy is represented in Figure 5.2 as well. The parameters,  $T_{ch} = 166 \pm 3.8$  MeV and  $T_{ch} = 173 \pm 5.8$  MeV are extracted from the analysis of STAR data in dAu collisions and in AuAu collisions at the energy of 200 GeV, respectively. Also,  $T_{ch} = 146 \pm 4$  MeV is from the analysis of ALICE data in pp collisions at  $\sqrt{s} = 900$  GeV and  $T_{ch} = 163 \pm 0.5$  MeV is from the analysis of ALICE data in PbPb collisions at  $\sqrt{s_{NN}} = 2.76$  TeV.

At this point, we believe a reference study will make a significant contribution to the evaluation of the relations above. The plot given in Figure 5.3 [69] includes two curves fitting the energy dependencies of two chemical freeze-out parameters,  $T$  and  $\mu_B$ , individually. The curves in both two sections (lower and upper), the upper section has an increasing tendency with the temperature whereas the lower one is opposite. All the data calculated from various accelerators in the lower energy regime are shown with different colored legends in Figure 5.3. Although the energy scale is arranged purely for heavy-ion collisions, Figure 5.3 can help to give the general trend of the plots given in Figure 5.1 and Figure 5.2.

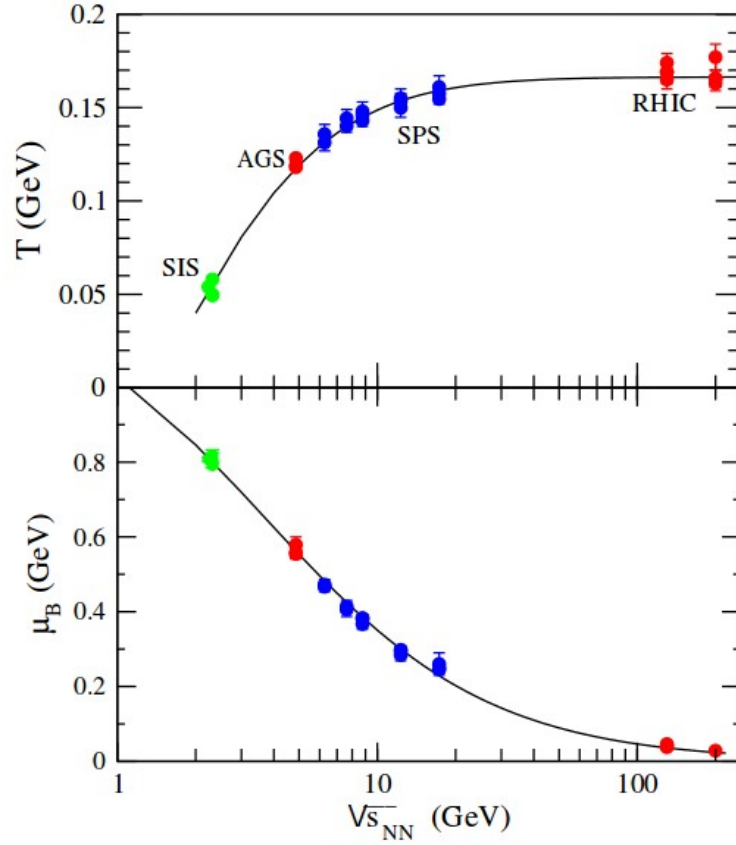


**Figure 5.3:** The upper and the lower section showing the energy dependencies of  $T$  and  $\mu_B$  in heavy-ion collisions, respectively [69].

The THERMUS results from both Figure 5.1 and Figure 5.2 can be used to extend the energy scale of readily available in Figure 5.3. Using the data point for the energy of 2.76 TeV looks possible for extrapolating the center of mass energy. The plot showing the extrapolation of the center of mass energy is given in Figure 5.4. However, only the points where the results from heavy-ion collisions are included into the extension

which leads the energy scale to be 2.76 TeV. The two data points taken from the analysis of 200 GeV center of mass energy are included to verify our results if they correspond to the previous results.

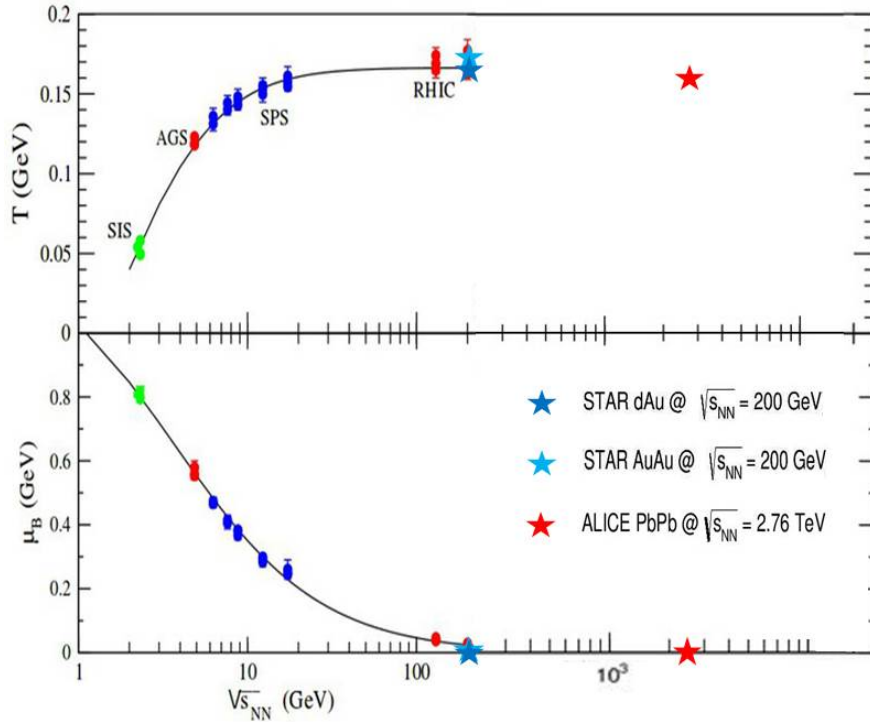


**Figure 5.4:** The extended version of the plot shown in Figure 5.3. The upper and the lower section again showing the energy dependencies of  $T$  and  $\mu_B$  in heavy-ion collisions, respectively.

The agreement between available data and results from the THERMUS calculations in this thesis looks very good. New data between the energies of 200 GeV and 2.76 TeV is a wonder if the results from those are consistent with the extrapolated value of the curve between these energies.

## 6. CONCLUSION AND OUTLOOK

In the analysis presented in chapter 4, the statistical-thermal parameters are determined at the chemical freeze-out point which gives information about the QGP medium. Recalling space-time evolution of strongly interacting matter in Figure 2.1, the hadronic particles can escape from the medium and be detected by the experimental setup above the freeze-out limit. ALICE Physics is deeply interested in the particles released above the freeze-out limit since it is believed that these particles carry information about the medium where the collisions take place. Therefore, it is thought that these statistical-thermal model analysis are quite valuable for both future theoretical and experimental studies. Also, the studies conducted in this thesis show that strangeness canonical ensemble which is widely used in such a large-scale is successful in describing nearly all the collision systems.

As a next step, since the ALICE data at higher energies is still on progress and the experimental particle ratios are not available yet, the predictions of statistical-thermal approach relevant to these ratios are the studies beneficial for future work. In this work, only the temperature dependencies of the statistical-thermal parameters are presented. However, it is certain that the precise determination of the relations between all the statistical-thermal parameters increase the maturity of the level of the analysis. As it was given in the previous section, the feed-down contribution is a method of improving the results of the ratios which does not correspond to experimental data. The inaccurate predictions of  $\Sigma^*$  and  $\rho^0$  in THERMUS which are previously explained might be improved by feed-down correction. This is one of the future project planned to study on. The further studies mentioned above may lead to put forward effective and pioneering physical outcome in the future.



## REFERENCES

- [1] **Lettesier, J. and Rafelski J.** (2002). *Hadrons and Quark-Gluon Plasma*, Cambridge University Press.
- [2] **Kraus, I., Cleymans, J., Oeschler, H., Redlich, K., and Wheaton, S.,** (2006). Statistical Model Predictions for Pb–Pb Collisions at LHC, *J. Phys. G: Nucl. Part. Phys.*, **32**, 495–498.
- [3] **Griffiths, D. J.** (1942). *Introduction to Elementary Particles*, John Wiley & Sons, Inc.
- [4] **Friman, B., Höhne, C., Knoll, J., Leupold, S., Randrup, J., Rapp, R. and Senger, P.** (2011). *The CBM Physics Book-Compressed Baryonic Matter in Laboratory Experiments*, Springer Publishing.
- [5] **Amsler, C. vd.[Particle Data Group]**, (2008). Review of Particle Physics, *Phys. Lett. B*, **667**, (1-5):1-1340.
- [6] **Halzen, F. and Martin A.D.** (1984). *Quarks and Leptons*, Springer.
- [7] **Tiwari, K. and Singh C. P.**,(2012). Particle Production in Ultra-relativistic Heavy-Ion Collisions: A Statistical-Thermal Model Review, *Phys. Rev. D*, arXiv:1306. 3291 [hep-th].
- [8] **Bjorken, J. D.**,(1983). Highly Relativistic Nucleus-Nucleus Collisions: The Central Rapidity Region, *Phys. Rev. D*, **27**, 140.
- [9] **Karasu Uysal, A.** (2011). Study of  $K_s^0$ ,  $\bar{\Lambda}_0$ ,  $\Lambda_0$  and  $\Delta^{++}$  (1232) and  $\Delta^{--}$  (1232) Productions in pp Collisions at 7 TeV with the ALICE *Ph.D. thesis*, Yıldız Technical University, Turkey.
- [10] **Rafelski, J. and Muller, B.**, (1982). Strangeness Production in the Quark-Gluon Plasma, *Phys. Rev. Lett.*, **48**, 1066-1069.
- [11] **Alexopoulos, T. vd.**, (2002). Evidence for Hadronic Deconfinement in Anti-p p Collisions at 1.8 TeV, *Phys. Lett. B*, **528**, 43-48.
- [12] **Wheaton, S., Cleymans, J. and Hauer, M.**, (2009). THERMUS - A Thermal Model Package for ROOT, *Com. Phys. Commun.*, **180**, 84-106.
- [13] **Salur, S. (for the STAR Collaboration)** (2006). Statistical Models and STAR's Strange Data, *22nd Winter Workshop on Nuclear Dynamics Talk Proceedings*, arXiv:nucl-ex/0606006.

- [14] **Floris, M. (for the ALICE Collaboration)**, (2002). Identified Particles in pp and Pb-Pb Collisions at LHC Energies with the ALICE Detector, *Plenary talk at Quark Matter 2011, May 23rd-28th 2011, Annecy, France*, arXiv:1108.3257 [hep-ex].
- [15] **Abelev, B. (for the ALICE Collaboration)**, (2012). Strangeness with ALICE: from pp to Pb-Pb, *Proceedings for the Physics of the LHC 2012 Conference, in Vancouver, BC*, arXiv:1209.3285 [nucl-ex].
- [16] **Dokshitzer, Yu. L., Khoze, V. A., Mueller, A. H. and Troyan, S. I.** (1989). *Basics of Perturbative QCD*, World Scientific Publishing, Singapore.
- [17] **Capella A., Sukhatme, U., Tan, C. and Tran Thanh Van, J.**, (1994). Dual Parton Model, *Phys. Rept.*, **236**, 225–329.
- [18] **Engel, R. and Ranft, J.**, (1996). Hadronic Photon-Photon Interactions at High Energies, *Phys. Rev.D*, **54**, 4244–4262.
- [19] **Sjostrand T., Lonnblad L., Mrenna S. and Skands, P.**, (2001). Pythia 6.2: Physics and Manual, arXiv:hep-ph/01088264.
- [20] **Koppe, H.**, (1949). On the Production of Mesons, *Phys. Rev.*, **76**, 688.
- [21] **Hagedorn, R.**, (1965). Statistical Thermodynamics of Strong Interactions at High-Energies, *Nuovo Cim.Suppl.*, **3**, (147-186).
- [22] **Braun-Munzinger P., Redlich K. and Stachel, J.** (2004). *Quark Gluon Plasma 3*, Hwa R. and Wang X., World Scientific Publishing, Singapore.
- [23] **Redlich, K., Cleymans, J., Oeschler, H. and Tounsi, A.**, (2002). Particle Production and Equilibration in Heavy Ion Collisions, *Acta Phys. Pol. B*, **33,6**,1609-1628.
- [24] **Letessier, J. and Rafelski, J.**, (2008). Hadron Production and Phase Changes in Relativistic Heavy Ion Collisions, *Eur. Phys. J. A*, **35,2**,221-242.
- [25] **Wheaton, S.**, (2005). Overview of the Statistical-Thermal Model as Applicable to THERMUS.
- [26] **Braun-Munzinger P., Heppel, I. and Stachel, J.**, (1999). Chemical Equilibration in Pb+Pb collisions at the SPS, *Phys. Lett. B*, **465**, 15.
- [27] **Broniowski, W. and Florkowski, W.**, (2002). Geometric Relation Between Centrality and the Impact Parameter in Relativistic Heavy-Ion Collisions, *Phys. Rev. C*, **65**, 064905.
- [28] **Kaneta, K. (for the NA44 Collaboration)**, (1997). Particle Ratios from Central Pb + Pb Collisions at the CERN SPS, *J. Phys. G: Nucl. Part. Phys.*, **23**, 1865.
- [29] **Redlich, K., Cleymans, J., Oeschler, H. and Tounsi, A.**, (2001). Conservation Law and Particle Production in Heavy Ion Collisions, arXiv:hep-ph/0110337.

- [30] **Cleymans, J., Kraus, I., Redlich, K. and Wheaton, S.**, (2006). Statistical Model Predictions for Particle Ratios at  $\sqrt{s_{NN}} = 5.5$  TeV, *Phys.Rev. C*, **74**, (034903).
- [31] **Becattini, F. and Heinz, U.**, (1997). Thermal Hadron Production in pp and p $\bar{p}$  Collisions, *Z Phys. C*, **76**, 269.
- [32] **Cleymans, J., Elliott, D., Kernen, A. and Suhonen, E.**, (1998). Thermal Model Analysis of Particle Ratios in Ni+Ni Experiments Using Exact Strangeness Conservation, *Phys. Rev. C*, **57**, 3319.
- [33] **Becattini, F., Kampfer, B., Kaneta, M., Wheaton, S. and Xu, N.**, (2005). Centrality Dependence of Thermal Parameters Deduced from Hadron Multiplicities in Au+Au Collisions at  $\sqrt{s_{NN}}=130$ GeV, *Phys. Rev. C*, **71**, 054901.
- [34] **Becattini, F., Gazdzicki, M., Kernen, A., Mannien, J. and Stock, R.**, (2004). Chemical Equilibrium Study in Nucleus-Nucleus Collisions at Relativistic Energies, *Phys. Rev. C*, **69**, 024905.
- [35] **Bearden, I. G., et al. (NA44)**, (2002). Particle Production in Central Pb+Pb Collisions at 158 A GeV/c, *Phys. Rev. C*, **66**, 044907.
- [36] **Cleymans, J., Kmpfer, B. and Wheaton, S.**, (2002). Centrality Dependence of Thermal Parameters in Heavy-Ion Collisions at Relativistic Energies, *Phys. Rev. C*, **65**, 027901, arXiv:nucl-th/0110035.
- [37] **Cleymans, J., Kmpfer, B. and Wheaton, S.**, (2003). Towards Strangeness Saturation in Central Heavy Ion Collisions at High Energies, *Nucl. Phys. A*, **715**, 553, arXiv:hep-ph/0208247.
- [38] **Cleymans, J., Kmpfer, B., Steinberg, P. and Wheaton, S.**, (2004). System-size Dependence of Strangeness Saturation, *J. Phys. G: Nucl. Part. Phys.*, **30**, 595, arXiv:hep-ph/031020.
- [39] **Kraus, I., Cleymans, J., Oeschler, H., Redlich, K. and Wheaton, S.**, (2009). Statistical Model Predictions for p+p and Pb+Pb Collisions at LHC, arXiv:0902.0873 [hep-ph].
- [40] **Kraus, I., Cleymans, J., Oeschler H., Redlich, K. and Wheaton, S.**, (2007). Chemical Equilibrium in Collisions of Small Systems, *Phys. Rev. C*, **76**, (064903).
- [41] **Cleymans, J. et al.**, (2004). System-size Dependence of Strangeness Saturation, *J. Phys. G: Nucl. Part. Phys.*, **30**, (S595).
- [42] **Becattini, F., Cleymans, J., Keranen, A., Suhonen, E. and Redlich, K.**, (2001). Features of Particle Multiplicities and Strangeness Production in Central Heavy Ion Collisions between 1.7A and 158A GeV/c, *Phys.Rev. C*, **64**, (024901).

- [43] **Andronic, A., Braun-Munzinger P. and Stachel, J.**, (2006). Hadron Production in Central Nucleus-Nucleus Collisions at Chemical Freeze-out, *Nucl. Phys. A*, **772**, 167.
- [44] **Cleymans, J., Oeschler, H., Redlich, K. and Wheaton, S.**, (2006). Comparison of Chemical Freeze-out Criteria in Heavy-Ion Collisions, *Phys. Rev. C*, **73**, 034905.
- [45] **Becattini, F., Manninen, J. and Gazdzicki, M.**, (2006). Energy and System Size Dependence of Chemical Freeze-out in Relativistic Nuclear Collisions, *Phys. Rev. C*, **73**, 044905.
- [46] **Torrieri, G., Steinke, S., Broniowski, W., Florkowski, W., Letessier, J. and Rafelski, J.**, (2005). SHARE: Statistical Hadronization with Resonances, *Comput. Phys. Commun.*, **167**, 229.
- [47] **Torrieri, G., Jeon, S., Letessier, J. and Rafelski, J.**, (2006). SHAREv2: Fluctuations and a Comprehensive Treatment of Decay Feed-down, *Comput. Phys. Commun.*, **175**, 635.
- [48] **Caines, H.**, (2006). Using strange hadrons as probes of dense matter, *J. Phys. G*, **32**, 171.
- [49] **Stiles, L.A. and Murray, M.**, (2006). Limiting fragmentation of chemical potentials in heavy ion collisions, arXiv:nucl-ex/0601039.
- [50] **Takahashi, J. (for the STAR Collaboration)**, (2007). Energy and System Size Dependence of Strangeness Production from SPS to RHIC, arXiv:nucl-ex/0711.2273.
- [51] **Murray, M. (for the BRAHMS Collaboration)**, (2007). Flavor Dynamics, arXiv:nucl-ex/0710.4576.
- [52] **Gorenstein, M.I., Hauer, M. and Moroz, O.N.**, (2007). Viscosity in the Excluded Volume Hadron Gas Model, arXiv:nucl-th/0708.0137.
- [53] **Witt, R.**, (2007).  $\Xi^0$  (1530) Production in Heavy-Ion Collisions Linebreak and its Implications for  $\Delta t_{(therm-chem)}$ , *J. Phys. G*, **34**, 921.
- [54] **Hippolyte, B.**, (2007).  $\Xi^0$ (1530) Strange prospects for LHC energies, *Eur. Phys. J. C*, **49**, 121.
- [55] **Cleymans, J., Sahoo, R., Mahapatra, D.P., Srivastava, D.K. and Wheaton, S.**, (2008).  $\Xi^0$  (1530) Transverse Energy per Charged Particle and Freeze-Out Criteria in Heavy-Ion Collisions, *Phys. Lett. B*, **660**, 172.
- [56] **Becattini, B., Manninen, J., Gazdzicki, M.**, (2006). Energy and System Size Dependence of Chemical Freeze-out in Relativistic Nuclear Collisions, *Phys. Rev. C*, **73**, 044905.

- [57] **James, F., Roos, M.**, (1975). Minit: A System for Function Minimization and Analysis of the Parameter Errors and Correlations, *Comput. Phys. Commun.*, **10**, 343-367.
- [58] **Glendenning, N.K. and Rafelski, J.**, (1985). Kaons and quark-gluon plasma, *Phys.Rev. C*, **31**, (823).
- [59] **Oeschler, H., Cleymans, J., Redlich, K. and Wheaton, S.**, (2006). Transition from Baryon- to Meson-Dominated Freeze Out -Early Decoupling around 30 A GeV? , *J. Phys. G*, **32**, (223-229).
- [60] **Cleymans, J., Kraus, I., Oeschler, H., Redlich, K. and Wheaton, S.** (2009). Statistical Model Predictions for p+p and Pb+Pb Collisions at LHC, arXiv:0902.0873 [hep-ph]
- [61] **Vernet, R. (for the collaboration)**, (2011). First measurements of strangeness production in pp collisions with the ALICE experiment at LHC, *Nuclear Physics B - Proceedings Supplements*, **210–211**, 221-242.
- [62] **B.I. Abelev, et al. (for STAR Collaboration)**, (2009). Systematic Measurements of Identified Particle Spectra in pp, d+Au and Au+Au Collisions from STAR, *Phys. Rev. C*, **79**, 034909.
- [63] **Abelev, B. I. et al. (STAR Collaboration)**, (2008). Hadronic Resonance Production in d+Au Collisions at  $\sqrt{s_{NN}} = 200$  GeV Measured at the BNL Relativistic Heavy Ion Collider, *Phys. Rev. C*, **78**, 044906.
- [64] **Bratkovskaya, E. L., Konchakovski, V. P., Voronyuk, V., Toneev, V. D., Linnyk, O. and Cassing, W.**, (2012). The QGP phase in relativistic heavy-ion collisions, *Proceedings of the International Symposium on 'Exciting Physics', Makutsi-Range, South Africa, 13-20 November, 2011* arXiv:1202.4891 [nucl-th].
- [65] **ALICE Collaboration**, (2011). Production of Pions, Kaons and Protons in pp Collisions at  $\sqrt{s} = 900$  GeV with ALICE at the LHC, *Eur. Phys. J. C*, **71**, 1655.
- [66] **Abelev, B. (for the ALICE Collaboration)**, (2012). Pion, Kaon, and Proton Production in Central PbPb Collisions at  $\sqrt{s_{NN}} = 2.76$  TeV, *Phys. Rev. Lett.*, **109**, 252301.
- [67] **ALICE Collaboration**, (2013).  $K_S^0$  and  $\Lambda$  production in Pb-Pb collisions at  $\sqrt{s_{NN}} = 2.76$  TeV, *Phys. Rev. Lett.*, **111**, 222301.
- [68] **ALICE Collaboration**, (2014). Multi-strange baryon production at mid-rapidity in Pb-Pb collisions at  $\sqrt{s_{NN}} = 2.76$  TeV, *Phys. Lett. B* **216**, 728.
- [69] **Cleymans, J., Oeschler, H., Redlich, K. and Wheaton, S.**, (2006). Comparison of Chemical Freeze-Out Criteria in Heavy-Ion Collisions, *Phys.Rev.C*, **73**, 034905, arXiv:hep-ph/0511094.



## **CURRICULUM VITAE**

**Name Surname: ıđdem Yařar**

**Place and Date of Birth: Istanbul - 04.01.1984**

**E-Mail: cyasar@itu.edu.tr**

**B.Sc.: Yıldız Technical University- Physics Department, 3.42/4.00**

**M.Sc.: Istanbul Technical University- Physics Engineering Programme, 3.50/4.00**

**Fellowships: The Scientific and Technological Research Council of Turkey (TUBITAK) 2211 National Graduate Scholarship Programme, 11.2013-06.2014.**

**Research Project Participation: The Scientific and Technological Research Council of Turkey (TUBITAK) 3501 National Young Researchers Career Development Programme, volunteer M.S. Student.**

**Publications: I- Turkish Physical Society 30th International Physics Congress, poster presentation, Thermal Model Description of Hadron Yields, 2013.**

**II- İzmir High Energy Physics Workshop (İZYEF), poster presentation, ALICE Experiment, 2013.**